Quantum four-stroke heat engine: Thermodynamic observables in a model with intrinsic friction

Tova Feldmann and Ronnie Kosloff*
Department of Physical Chemistry, The Hebrew University, Jerusalem 91904, Israel
(Received 11 February 2003; published 3 July 2003)

The fundamentals of a quantum heat engine are derived from first principles. The study is based on the equation of motion of a minimum set of operators, which is then used to define the state of the system. The relation between the quantum framework and the thermodynamical observables is examined. A four-stroke heat engine model with a coupled two-level system as a working fluid is used to explore the fundamental relations. In the model used, the internal Hamiltonian does not commute with the external control field, which defines the two adiabatic branches. Heat is transferred to the working fluid by coupling to hot and cold reservoirs under constant field values. Explicit quantum equations of motion for the relevant observables are derived on all branches. The dynamics on the heat transfer constant field branches is solved in closed form. On the adiabats, a general numerical solution is used and compared with a particular analytic solution. These solutions are combined to construct the cycle of operation. The engine is then analyzed in terms of the frequency-entropy and entropy-temperature graphs. The irreversible nature of the engine is the result of finite heat transfer rates and frictionlike behavior due to noncommutability of the internal and external Hamiltonians.

DOI: 10.1103/PhysRevE.68.016101 PACS number(s): 05.70.Ln, 07.20.Pe

I. INTRODUCTION

Analysis of heat engine models has been a major part of thermodynamic development. For example, Carnot's engine preceded the concepts of energy and entropy [1]. Szilard and Brillouin constructed a model engine that enabled them to resolve the paradox raised by Maxwell's demon [2,3]. The subsequent insight enabled the unification of negative entropy with information. In the same tradition, in the present paper, we study a heat engine model with a quantum working fluid for the purpose of tracing the microscopic origin of friction. The function of a quantum heat engine, as well as its classical counterpart, is to transform heat into useful work. In such engines, the work is extracted by an external field exploiting the spontaneous flow of heat from a hot to a cold reservoir. The present model performs this task by a four-stroke cycle of operation. All four branches of the cycle can be described by quantum equations of motion. The thermodynamical consequences can therefore be derived from first principles.

The present paper lays the foundation for a comprehensive analysis of a discrete model of a quantum heat engine. A brief outline, which has been published, emphasized the engine's optimal performance characteristics [4]. It was shown that the engines power output versus cycle time mimics very closely a classical heat engine subject to friction. The source of the apparent friction was traced back to a quantum phenomena: the noncommutability of the external control field Hamiltonian and the internal Hamiltonian of the working medium.

The fundamental issue involved requires a detailed and careful study. The approach followed is to derive the thermodynamical concepts from quantum principles. The connecting bridges are the quantum thermodynamical observables. Following the tradition of Gibbs, a minimum set of observables is sought, which are sufficient to characterize the performance of the engine. When the working fluid is in thermal equilibrium, the energy observable is sufficient to completely describe the state of the system and therefore all other observables. During the cycle of operation, the working fluid is in a nonequilibrium state. In frictionless engines, where the internal Hamiltonian commutes with the external control field, the energy observable is still sufficient to characterize the engine's cycle [5,6]. In the general case, additional variables have to be added. For example, in the current model, a set of three quantum thermodynamic observables is sufficient to characterize the performance. With only two additional variables, the state of the working fluid can be characterized also. Knowledge of the state is necessary in order to evaluate the entropy and the dynamical temperature. These variables are crucial in establishing a thermodynamic perspective.

The current investigation is in line with previous studies of quantum heat engines [4–18]. All the studies of first-principle quantum models have conformed to the laws of thermodynamics. These models have been either continuous resembling turbines [12,16,17], or discrete as in the present model [4,5,10–12]. Surprisingly, the performance characteristics of the models were in close resemblance to their realistic counterparts. Real heat engines operate far from the reversible conditions, where the maximum power is restricted due to finite heat transfer [19], internal friction, and heat leaks [20–26]. Analysis of the quantum models of heat engines, based on a first-principle dynamical theory, enables to pinpoint the fundamental origins of finite heat transfer, internal friction, and heat leaks.

Studies of quantum continuous heat engine models have revealed most of the known characteristics of real engines. In accordance with finite-time thermodynamics, the power always exhibits a definite maximum [21], and the performance has been limited by heat leaks [17]. Finally, indications of restrictions due to frictionlike phenomena have been indicated [12]. The difficulty with the analysis is that it is very

*Electronic address: ronnie@fh.huji.ac.il

hard to separate the individual contributions in the case of a continuous operating engine.

To facilitate the interpretation, a four-stroke discrete engine has been chosen for analysis. The cycle of operation is controlled by the segments of time that the engine is in contact with a hot and a cold bath, and by the time interval required to vary the external field. To simplify the analysis, the time segments where the working fluid is in contact with the heat baths are carried out at constant external field. Such a cycle of operation resembles the Otto cycle, which is composed of two *isochores* where heat is transferred and two *adiabats* where work is done. This simplification allows us to obtain the values of the thermodynamical observables during the cycle of operation from first principles in closed form.

II. QUANTUM THERMODYNAMICAL OBSERVABLES AND THEIR DYNAMICS

The quantum thermodynamical observables constitute a set of variables, which are sufficient to completely describe the heat engine performance characteristics as well as the entropy and temperature changes of its working medium. The analysis of the performance requires a quantum dynamical description of the changes in the thermodynamical observables during the engine's cycle of operation. The thermodynamical observables are associated with the expectation values of operators of the working medium. Using the formalism of von Neumann, an expectation value of an observable $\langle\hat{\mathbf{A}}\rangle$ is defined by the scalar product of the operator $\hat{\mathbf{A}}$ representing the observable and the density operator $\hat{\boldsymbol{\rho}}$ representing the state of the working medium:

$$\langle\hat{\mathbf{A}}\rangle=(\hat{\mathbf{A}}\cdot\hat{\boldsymbol{\rho}})=\mathrm{Tr}\{\hat{\mathbf{A}}^{\dagger}\hat{\boldsymbol{\rho}}\}. \tag{1}$$

The dynamics of the working medium is subject to the external change of variables as well as heat transport from the hot and to the cold reservoir. The dynamics is then described within the formulation of quantum open systems [28,32], where the dynamics is generated by the Liouville superoperator $\mathcal{L}$ either as an equation of motion for the state $\boldsymbol{\rho}$ (Schrödinger picture),

$$\dot{\hat{\boldsymbol{\rho}}}=\mathcal{L}(\hat{\boldsymbol{\rho}}), \tag{2}$$

or as an equation of motion for the operator (Heisenberg picture),

$$\dot{\hat{\mathbf{A}}}=\mathcal{L}^{*}(\hat{\mathbf{A}})+\frac{\partial\hat{\mathbf{A}}}{\partial t}. \tag{3}$$

The second part of the right-hand side (rhs) appears since the operator $\hat{\mathbf{A}}$ can be explicitly time dependent.

A significant simplification is obtained [27] when the following conditions are met.

(a) The operators of interest form an orthogonal set $\hat{\mathbf{B}}_{\mathbf{i}}$ i.e.,

$$(\hat{\mathbf{B}}_{\mathbf{i}}\cdot\hat{\mathbf{B}}_{\mathbf{j}})=\delta_{\mathbf{ij}}, \tag{4}$$

where $\hat{\mathbf{B}}_0=\hat{\mathbf{I}}$ is the identity operator. Then, the set $\hat{\mathbf{B}}_{\mathbf{i}}$ for the Hilbert space a nd will be used as a basis.

(b) The set is closed to the operation of $\mathcal{L}^{*}$:

$$\dot{\hat{\mathbf{B}}}_{\mathbf{i}}=\mathcal{L}^{*}(\hat{\mathbf{B}}_{\mathbf{i}})=\sum_{\mathbf{j}} l_{\mathbf{j}}^{\mathbf{i}}\hat{\mathbf{B}}_{\mathbf{j}}, \tag{5}$$

where $l_{\mathbf{i}}^{\mathbf{j}}$ are scalar coefficients composing the matrix $\tilde{L}$.

(c) The equilibrium density operator is a linear combination of the set

$$\hat{\boldsymbol{\rho}}^{eq}=\frac{1}{N}\hat{\mathbf{I}}+\sum_{\mathbf{k}} b_{\mathbf{k}}^{eq}\hat{\mathbf{B}}_{\mathbf{k}}, \tag{6}$$

where N is the dimension of the Hilbert space and $b_{\mathbf{k}}^{eq}$ are the equilibrium expectation values of operators, $\langle\hat{\mathbf{B}}_{\mathbf{k}}{}^{eq}\rangle$.

The operator property of Eq. (5) allows a direct solution to the Heisenberg equation of motion (3) by diagonalizing the $\tilde{L}$ matrix, relating observables $\langle\hat{\mathbf{B}}_{\mathbf{k}}\rangle$ at time t to observables at time $t+\Delta t$, that is, $\vec{\mathbf{b}}(t+\Delta t)=\mathcal{U}(\Delta t)\vec{\mathbf{b}}(t)$, where $\mathcal{U}=e^{\tilde{L}\Delta t}$ and $\vec{\mathbf{b}}$ is a vector composed from the expectation values of $\hat{\mathbf{B}}_{\mathbf{k}}$ [for an example, cf. Eq. (35)].

The time-dependent expectation values $\vec{\mathbf{b}}(t)$ and Eq. (6) can be employed to reconstruct the density operator

$$\hat{\boldsymbol{\rho}}^{R}=\frac{1}{N}\hat{\mathbf{I}}+\sum_{\mathbf{k}} b_{\mathbf{k}}\hat{\mathbf{B}}_{\mathbf{k}}, \tag{7}$$

where the expansion coefficients become $b_{\mathbf{k}}=\langle\hat{\mathbf{B}}_{\mathbf{k}}\rangle$. Although the set $\hat{\mathbf{B}}_{\mathbf{k}}$ is not necessarily complete, Eq. (7) will still be used as a reconstructing method for the density operator. This reconstructed state $\hat{\boldsymbol{\rho}}^{R}$ reproduces all observations that are constructed from linear combinations of the set of operators $\hat{\mathbf{B}}_{\mathbf{k}}$. The reconstruction of the density operator $\hat{\boldsymbol{\rho}}^{R}$ means that the dynamics can be solved in the Heisenberg frame, Eq. (3). When the state of the system is required, for example, in entropy calculations (cf. Sec. II B), the reconstructed state $\hat{\boldsymbol{\rho}}^{R}$ is sufficient.

The Liouville operator, Eqs. (2) and (3), for an open quantum system can be partitioned into a unitary part $\mathcal{L}_H$ and a dissipative part $\mathcal{L}_D$ [28]:

$$\mathcal{L}=\mathcal{L}_H+\mathcal{L}_D. \tag{8}$$

The unitary part is generated by the Hamiltonian $\hat{\mathbf{H}}$:

$$\mathcal{L}_H^{*}(\hat{\mathbf{A}})=i[\hat{\mathbf{H}},\hat{\mathbf{A}}]. \tag{9}$$

The condition for a set of operators to be closed under $\mathcal{L}_H^{*}$ has been well studied [29]. If the Hamiltonian can be decomposed to

$$\hat{\mathbf{H}}=\sum_{\mathbf{j}} h_{\mathbf{j}}\hat{\mathbf{B}}_{\mathbf{j}}, \tag{10}$$

and the set $\hat{\mathbf{B}}_\mathbf{k}$ forms a Lie algebra [30,31], i.e., $[\hat{\mathbf{B}}_\mathbf{i},\hat{\mathbf{B}}_\mathbf{j}]=\Sigma_\mathbf{k} C_\mathbf{ij}^\mathbf{k}\hat{\mathbf{B}}_\mathbf{k}$ (the coefficients $C_\mathbf{ij}^\mathbf{k}$ are the structure factors of the Lie algebra), then the set is closed under $\mathcal{L}_H^*$.

For the dissipative Liouville operator $\mathcal{L}_D$, Lindblad's form is used [28]:

$$\mathcal{L}_D^*(\hat{\mathbf{A}})=\sum_\mathbf{j}\left[\hat{\mathbf{F}}_\mathbf{j}\hat{\mathbf{A}}\hat{\mathbf{F}}_\mathbf{j}^\dagger-\frac{1}{2}(\hat{\mathbf{F}}_\mathbf{j}\hat{\mathbf{F}}_\mathbf{j}^\dagger\hat{\mathbf{A}}+\hat{\mathbf{A}}\hat{\mathbf{F}}_\mathbf{j}\hat{\mathbf{F}}_\mathbf{j}^\dagger)\right], \tag{11}$$

where $\hat{\mathbf{F}}_\mathrm{j}$ are operators from the Hilbert space of the system. The conditions for which the set $\hat{\mathbf{B}}_\mathbf{i}$ is closed to $\mathcal{L}_D^*$ have not been well established. Nevertheless, in the present studied example, such a set has been found.

A. Energy balance

The energy balance of the working medium is followed by the changes in time to the expectation value of the Hamiltonian operator. For a working medium, composed of a gas of interacting particles, the Hamiltonian is described as

$$\hat{\mathbf{H}}=\hat{\mathbf{H}}_\mathbf{ext}+\hat{\mathbf{H}}_\mathbf{int}. \tag{12}$$

Here, $\hat{\mathbf{H}}_\mathbf{ext}=\omega\Sigma_i\hat{\mathbf{H}}_\mathbf{i}$ is the sum of single-particle Hamiltonians, where $\omega=\omega(t)$ is the time dependent external field. It, therefore, constitutes the external control of the engine's operation cycle. $\hat{\mathbf{H}}_\mathbf{int}$ represents the uncontrolled interparticle interaction part.

The existence of the interaction term in the Hamiltonian means that the external field only partly controls the energy of the system. One can distinguish two cases, first case occurs when the two parts of the Hamiltonian $\hat{\mathbf{H}}_\mathbf{ext}$ and $\hat{\mathbf{H}}_\mathbf{int}$ commute. The other case occurs when $[\hat{\mathbf{H}}_\mathbf{ext},\hat{\mathbf{H}}_\mathbf{int}]\neq 0$ leads to $[\hat{\mathbf{H}}_\mathbf{int}(t),\hat{\mathbf{H}}_\mathbf{int}(t')]\neq 0$, causing important restrictions on the cycle of operation (cf. Sec. VI).

Since the energy is $E=\langle\hat{\mathbf{H}}\rangle$, the energy balance becomes, cf. Eq. (3):

$$\frac{dE}{dt}=\langle\mathcal{L}^*(\hat{\mathbf{H}})\rangle+\left\langle\frac{\partial\hat{\mathbf{H}}}{\partial t}\right\rangle. \tag{13}$$

Equation (13) is composed of the change in time due to the explicit time dependence of the Hamiltonian [cf. Eq. (3)] interpreted as the thermodynamic power:

$$\mathcal{P}=\dot{\omega}\sum_i\langle\hat{\mathbf{H}}_\mathbf{i}\rangle, \tag{14}$$

where $\langle\hat{\mathbf{H}}_\mathbf{i}\rangle$ is the expectation value of the single-particle Hamiltonian. The accumulated work on an engine trajectory $\mathcal{W}=\int\mathcal{P}dt$.

The heat flow represents the change in energy due to dissipation:

$$\dot{\mathcal{Q}}=\langle\mathcal{L}_D^*(\hat{\mathbf{H}})\rangle=\langle\mathcal{L}_D^*(\hat{\mathbf{H}}_\mathbf{ext}+\hat{\mathbf{H}}_\mathbf{int})\rangle, \tag{15}$$

[note $\mathcal{L}^*(\hat{\mathbf{H}})=\mathcal{L}_D^*(\hat{\mathbf{H}})$ since $\mathcal{L}_H^*(\hat{\mathbf{H}})=0$]. Equations (13), (14), and (15) lead to the time derivative of the first law of thermodynamics [9,16,33,34]:

$$\frac{dE}{dt}=\mathcal{P}+\dot{\mathcal{Q}}. \tag{16}$$

B. Entropy balance

Assuming the bath is large, the entropy production due to heat transfer from the system to the bath becomes

$$\mathcal{DS}=\frac{\dot{\mathcal{Q}}}{T}, \tag{17}$$

where T is the bath temperature.

Adopting the supposition that entropy is a measure of the dispersion of the measurement of an observable $\langle\hat{\mathbf{A}}\rangle$, we can label the entropy of the working medium according to the measurement applied i.e., $\mathcal{S}_{\hat{\mathbf{A}}}$. The probability of obtaining a particular ith measurement outcome is $p_i=\mathrm{tr}\{\hat{\mathbf{P}}_\mathbf{i}\hat{\boldsymbol{\rho}}\}$, where $\hat{\mathbf{P}}_\mathbf{i}=|i\rangle\langle i|$ are the projections of the ith eigenvalue of the operator $\hat{\mathbf{A}}$. The entropy associated with the measurement of $\hat{\mathbf{A}}$ becomes

$$\mathcal{S}_{\hat{\mathbf{A}}}=-\sum_i p_i\ln p_i. \tag{18}$$

The probabilities in Eq. (18) can be obtained from the diagonal elements of the density operator $\boldsymbol{\rho}$ in the eigenrepresentation of $\hat{\mathbf{A}}$. The entropy of the operator $\hat{\mathbf{A}}$, which leads to minimum dispersion (18), defines an invariant of the system termed the von Neumann entropy [35]:

$$\mathcal{S}_{VN}=-tr\{\hat{\boldsymbol{\rho}}\ln\hat{\boldsymbol{\rho}}\}, \tag{19}$$

$\mathcal{S}_{\hat{\mathbf{A}}}\geqslant\mathcal{S}_{VN}$ for all $\hat{\mathbf{A}}$. When $\mathcal{S}_{VN}=0$, the state is pure. The analysis of the energy entropy $\mathcal{S}_E=\mathcal{S}_{\hat{\mathbf{H}}}$ of the working fluid during the cycle of operation is a source of insight into the dynamics. It has the property $\mathcal{S}_E\geqslant\mathcal{S}_{VN}$ with equality when the $\boldsymbol{\rho}$ is diagonal in the energy representation, which is true in thermal equilibrium. Then,

$$\hat{\boldsymbol{\rho}}^{eq}=\frac{e^{-\beta\hat{\mathbf{H}}}}{Z}, \tag{20}$$

with $\beta=1/k_bT$ and $Z=\mathrm{tr}\{e^{-\beta\hat{\mathbf{H}}}\}$, The system's temperature has thus become identical to the bath temperature. When the working medium is not in thermal equilibrium, a dynamical temperature of the working medium is defined by [36]

$$T_{dyn}=\frac{\left\langle\frac{\partial E}{\partial t}\right\rangle}{\left\langle\frac{\partial\mathcal{S}_E}{\partial t}\right\rangle}, \tag{21}$$

where the derivative is taken with constant external field. Eq. (21) will be used to define the internal temperature of

the working fluid (cf. Sec. V A). The energy entropy $\mathcal{S}_E$ is used since the temperature is associated with the dispersion in energy. If the von Neumann entropy $\mathcal{S}_{vn}$ would have been used, the temperature would become infinite during unitary evolution stages.

III. THE QUANTUM MODEL

The following quantum model demonstrates a discrete heat engine with a cycle of operation defined by an external control on the Hamiltonian and by the time duration where the working medium is in contact with the hot and the cold bath. The model studied is a particular realization of the general framework of Sec. II. First, the generators of the motion, $\mathcal{L}_H$ and $\mathcal{L}_D$, are derived leading to equations of motion. These equations of motion are then solved for each of the branches, thus constructing the operating cycle.

A. The equations of motion

The generators of the equations of motion are the Hamiltonian for the unitary evolution and $\mathcal{L}_D$ for the dissipative part [cf. Eq. (8)]. The notation and normalization of the operators have been somewhat modified with respect to the notations of Ref. [4].

1. The Hamiltonian

The single-particle Hamiltonian is chosen to be proportional to the polarization of a two-level system (TLS), $\hat{\boldsymbol{\sigma}}_z^j$, which can be realized as an ensemble of spins in an external time dependent magnetic field. The operators $\hat{\boldsymbol{\sigma}}_z, \hat{\boldsymbol{\sigma}}_x, \hat{\boldsymbol{\sigma}}_y$ are the Pauli matrices. For this system, the external Hamiltonian, Eq. (12), becomes

$$\hat{\mathbf{H}}_{\mathbf{ext}} = 2^{-3/2}\omega(t)(\hat{\boldsymbol{\sigma}}_z^1 \otimes \hat{\mathbf{I}}^2 + \hat{\mathbf{I}}^1 \otimes \boldsymbol{\sigma}_z^2), \tag{22}$$

and the external control field $\omega(t)$ is chosen to be in the z direction.

The uncontrolled interaction Hamiltonian is chosen to be restricted to coupling of pairs of spin atoms. Therefore, the working fluid consists of noninteracting pairs of TLS's. For simplicity, a single pair can be considered. The thermodynamics of M pairs then follows by introducing a trivial scale factor. Accordingly, the uncontrolled part is

$$\hat{\mathbf{H}}_{\mathbf{int}} = 2^{-3/2}J(\hat{\boldsymbol{\sigma}}_x^1 \otimes \hat{\boldsymbol{\sigma}}_x^2 - \hat{\boldsymbol{\sigma}}_y^1 \otimes \hat{\boldsymbol{\sigma}}_y^2), \tag{23}$$

J scales the strength of the interaction. When $J \to 0$, the model represents a working medium with noninteracting atoms [5]. The interaction term, Eq. (23), defines a correlation energy between the two spins in the x and y directions. As a result, the interaction Hamiltonian does not commute with the external Hamiltonian, Eq. (22), which is chosen to be polarized in the z direction.

2. The operator algebra of the working medium

The maximum size of the complete operator algebra of two coupled spin systems is 16. A minimum set of operators closed to $\mathcal{L}^*$ is sought, which is sufficient as the basis for describing the thermodynamical quantities. First, a Lie algebra, which is closed to the unitary evolution part is to be determined. To generate this algebra, the commutation relations between the operators composing the Hamiltonian are evaluated [cf. Eq. (10)]. Defining

$$\hat{\mathbf{B}}_1 = 2^{-3/2}(\hat{\boldsymbol{\sigma}}_z^1 \otimes \hat{\mathbf{I}}^2 + \hat{\mathbf{I}}^1 \otimes \hat{\boldsymbol{\sigma}}_z^2) = \frac{1}{\sqrt{2}}\begin{pmatrix} 1 & 0 & 0 & 0 \\ 0 & 0 & 0 & 0 \\ 0 & 0 & 0 & 0 \\ 0 & 0 & 0 & -1 \end{pmatrix}, \tag{24}$$

where the tensor product eigenstates of $\hat{\boldsymbol{\sigma}}_z^1$ and $\hat{\boldsymbol{\sigma}}_z^2$ are used as a basis for the matrix representation, termed the ''polarization representation.'' Notice that $\hat{\mathbf{B}}_1$ is diagonal in this representation.

The second operator $\hat{\mathbf{B}}_2$ is

$$\hat{\mathbf{B}}_2 = 2^{-3/2}(\hat{\boldsymbol{\sigma}}_x^1 \otimes \hat{\boldsymbol{\sigma}}_x^2 - \hat{\boldsymbol{\sigma}}_y^1 \otimes \hat{\boldsymbol{\sigma}}_y^2) = \frac{1}{\sqrt{2}}\begin{pmatrix} 0 & 0 & 0 & 1 \\ 0 & 0 & 0 & 0 \\ 0 & 0 & 0 & 0 \\ 1 & 0 & 0 & 0 \end{pmatrix}. \tag{25}$$

The commutation relation $[\hat{\mathbf{B}}_1, \hat{\mathbf{B}}_2] = \sqrt{2}i\hat{\mathbf{B}}_3$ leads to the definition of $\hat{\mathbf{B}}_3$:

$$\hat{\mathbf{B}}_3 = 2^{-3/2}(\hat{\boldsymbol{\sigma}}_y^1 \otimes \hat{\boldsymbol{\sigma}}_x^2 + \hat{\boldsymbol{\sigma}}_x^1 \otimes \hat{\boldsymbol{\sigma}}_y^2)\frac{1}{\sqrt{2}}\begin{pmatrix} 0 & 0 & 0 & -i \\ 0 & 0 & 0 & 0 \\ 0 & 0 & 0 & 0 \\ i & 0 & 0 & 0 \end{pmatrix}. \tag{26}$$

The set of operators $\hat{\mathbf{B}}_1, \hat{\mathbf{B}}_2, \hat{\mathbf{B}}_3$ form a closed subalgebra of the total Lie algebra of the combined system. The Hamiltonian expressed in terms of the operators $\hat{\mathbf{B}}_1, \hat{\mathbf{B}}_2, \hat{\mathbf{B}}_3$ becomes

$$\hat{\mathbf{H}} = \omega\hat{\mathbf{B}}_1 + \mathrm{J}\hat{\mathbf{B}}_2 = \frac{1}{\sqrt{2}}\begin{pmatrix} \omega & 0 & 0 & J \\ 0 & 0 & 0 & 0 \\ 0 & 0 & 0 & 0 \\ J & 0 & 0 & -\omega \end{pmatrix}. \tag{27}$$

All the three operators are Hermitian, and orthogonal [cf. Eq. (4)]. Table I summarizes the commutation relations of this set of operators.

The commutation relations of the set of $\hat{\mathbf{B}}_\mathbf{k}$ operators define the SU(2) group and are isomorphic to the angular momentum commutation relations by the transformation $\hat{\mathbf{B}}_\mathbf{k} \to \hat{\mathbf{J}}_\mathbf{k}$. $\hat{\mathbf{B}}_1, \hat{\mathbf{B}}_2, \hat{\mathbf{B}}_3$ can be identified as the generators of rotations around the z,x, and y axes, respectively. This representation allows us to express the expectation values in a cartesian three-dimensional space (see Fig. 1).

TABLE I. Multiplication table of the commutation relations $[\hat{\mathbf{X}},\hat{\mathbf{Y}}]$ of the operators $\hat{\mathbf{B}}_1$, $\hat{\mathbf{B}}_2$, $\hat{\mathbf{B}}_3$, among themselves and with the Hamiltonian.

$\hat{\mathbf{X}}\backslash\hat{\mathbf{Y}}$	$\hat{\mathbf{B}}_1$	$\hat{\mathbf{B}}_2$	$\hat{\mathbf{B}}_3$
$\hat{\mathbf{B}}_1$	0	$i\sqrt{2}\mathbf{B}_3$	$-i\sqrt{2}\hat{\mathbf{B}}_2$
$\hat{\mathbf{B}}_2$	$-i\sqrt{2}\hat{\mathbf{B}}_3$	0	$i\sqrt{2}\hat{\mathbf{B}}_1$
$\hat{\mathbf{B}}_3$	$i\sqrt{2}\hat{\mathbf{B}}_2$	$-i\sqrt{2}\hat{\mathbf{B}}_1$	0
$\hat{\mathbf{H}}$	$-i\sqrt{2}\mathrm{J}\hat{\mathbf{B}}_3$	$i\sqrt{2}\omega\hat{\mathbf{B}}_3$	$i\sqrt{2}\mathrm{J}\hat{\mathbf{B}}_1-i\sqrt{2}\omega\hat{\mathbf{B}}_2$

3. The generators of the dissipative dynamics

The dissipative part of the dynamics is responsible for the approach to thermal equilibrium when the working medium is in contact with the hot (cold) baths. The choice of Lindblad's form in Eq. (11) guarantees the positivity of the evolution [28]. The operators $\hat{\mathbf{F}}_\mathrm{j}$ which lead to thermal equilibrium are constructed from the transition operators between the energy eigenstates. Diagonalizing the Hamiltonian (12) leads to the set of energy eigenvalues and eigenstates:

$$\epsilon_1=-\frac{\Omega}{\sqrt{2}},\quad \epsilon_2=0,\quad \epsilon_3=0,\quad \epsilon_4=\frac{\Omega}{\sqrt{2}},\tag{28}$$

where $\Omega=\sqrt{\omega^2+J^2}$. The method of construction of $\hat{\mathbf{F}}_\mathrm{j}$ is based on identifying the operators with the raising and lowering operators in the energy frame. For example, $\hat{\mathbf{F}}_1=\sqrt{k_\downarrow}|2\rangle\langle 1|$ or $\hat{\mathbf{F}}_2=\sqrt{k_\uparrow}|1\rangle\langle 2|$. The bath temperature enters through the detailed balance relation [5,10]

$$\frac{k_\uparrow}{k_\downarrow}=e^{-\beta\Omega/\sqrt{2}},\quad \beta=\frac{1}{T}.\tag{29}$$

The operators $\hat{\mathbf{F}}_\mathrm{j}$ constructed in the energy frame are then transformed into the polarization representation. The details are described in the Appendix. As can be seen in Sec. IV, this choice leads to the thermal equilibrium state.

Substituting the $\hat{\mathbf{B}}_\mathbf{i}$ operators into $\mathcal{L}_D$, Eq. (11), one gets

$$\mathcal{L}_D(\hat{\mathbf{B}}_1)=-\Gamma\left(\hat{\mathbf{B}}_1+\frac{\omega}{\sqrt{2}\Omega}\frac{k_\downarrow-k_\uparrow}{\Gamma}\hat{\mathbf{I}}\right),$$

$$\mathcal{L}_D(\hat{\mathbf{B}}_2)=-\Gamma\left(\hat{\mathbf{B}}_2+\frac{\mathrm{J}}{\sqrt{2}\Omega}\frac{k_\downarrow-k_\uparrow}{\Gamma}\hat{\mathbf{I}}\right),\tag{30}$$

$$\mathcal{L}_D(\hat{\mathbf{B}}_3)=-\Gamma(\hat{\mathbf{B}}_3),$$

where $\Gamma=k_\downarrow+k_\uparrow$.

From Eq. (30), the set of $\{\hat{\mathbf{B}}\}$ operators and the identity operator $\hat{\mathbf{I}}$ is closed with respect to the application of the dissipative operator $\mathcal{L}_D$ which leads to equilibration.

The interaction of the working medium with the bath can also be elastic. These encounters will scramble the phase conjugate to the energy of the system and are classified as pure dephasing (T_2) [cf. Eq. (83)]. In Lindblad's formulation, the dissipative generator of elastic encounters is described as

$$\mathcal{L}^*_{D^e}(\hat{\mathbf{A}})=-\gamma[\hat{\mathbf{H}},[\hat{\mathbf{H}},\hat{\mathbf{A}}]].\tag{31}$$

The elastic property is equivalent to $\mathcal{L}^*_{D^e}(\hat{\mathbf{H}})=0$. Moreover,

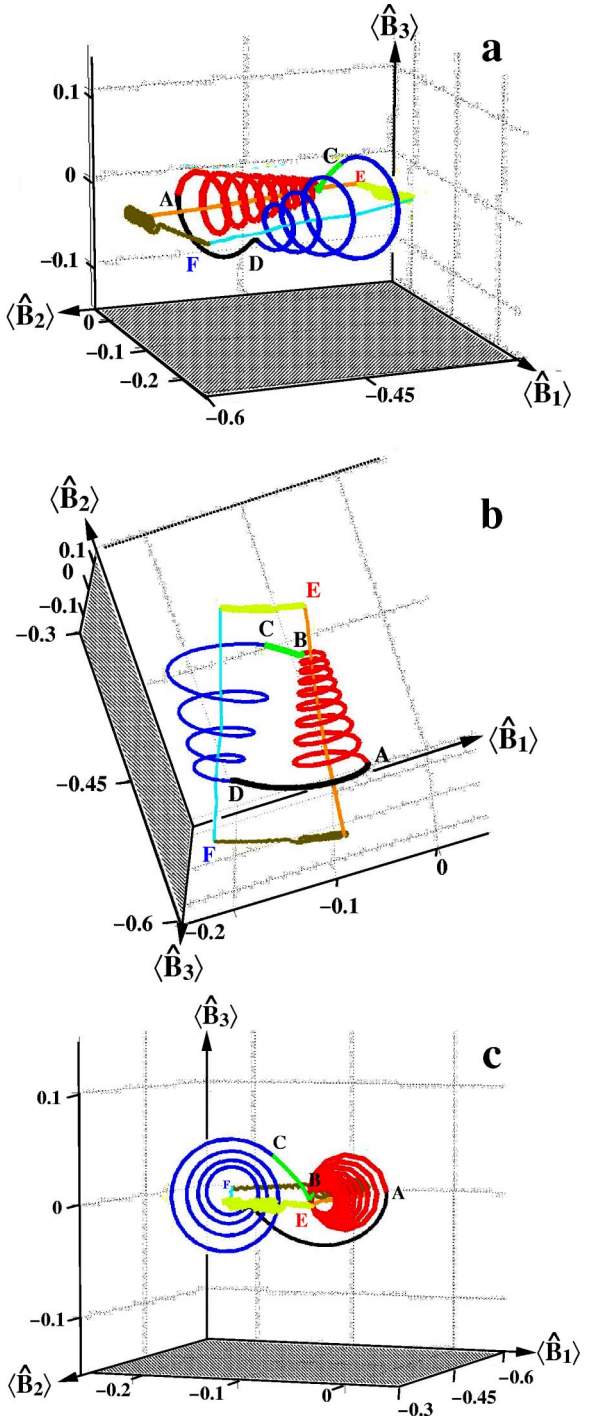

FIG. 1. The optimal cycle trajectory **ABCD** and the infinitely long trajectory **EF** in the $b_1=\langle\hat{\mathbf{B}}_1\rangle$, $b_2=\langle\hat{\mathbf{B}}_2\rangle$, $b_3=\langle\hat{\mathbf{B}}_3\rangle$ coordinate system showing three viewpoints.

the set $\hat{\mathbf{B}}_\mathbf{i}$ which is closed to the commutation relation with $\hat{\mathbf{H}}$ is also closed to $\mathcal{L}^*_{D^e}$.

To summarize, the set $\hat{\mathbf{B}}_\mathbf{1},\hat{\mathbf{B}}_\mathbf{2},\hat{\mathbf{B}}_\mathbf{3}$ and $\hat{\mathbf{I}}$ is closed under the operation of $\mathcal{L}^*=\mathcal{L}^*_H+\mathcal{L}^*_D+\mathcal{L}^*_{D^e}$. Gathering together the various contributions leads to the explicit form of the equation of motion

$$\frac{d}{dt}\begin{pmatrix}\langle\hat{\mathbf{B}}_\mathbf{1}\rangle\\ \langle\hat{\mathbf{B}}_\mathbf{2}\rangle\\ \langle\hat{\mathbf{B}}_\mathbf{3}\rangle\end{pmatrix} = \begin{pmatrix} -\Gamma-2\gamma J^2 & -2\gamma J\omega & \sqrt{2}J\\ -2\gamma\omega J & -\Gamma-2\gamma\omega^2 & -\sqrt{2}\omega\\ -\sqrt{2}J & \sqrt{2}\omega & -\Gamma-2\gamma\Omega^2\end{pmatrix} \times\begin{pmatrix}\langle\hat{\mathbf{B}}_\mathbf{1}\rangle\\ \langle\hat{\mathbf{B}}_\mathbf{2}\rangle\\ \langle\hat{\mathbf{B}}_\mathbf{3}\rangle\end{pmatrix} - \begin{pmatrix}\frac{\omega}{\sqrt{2}\Omega}(k_\downarrow-k_\uparrow)\\ \frac{J}{\sqrt{2}\Omega}(k_\downarrow-k_\uparrow)\\ 0\end{pmatrix} \tag{32}$$

or in vector form

$$\frac{d}{dt}\vec{\mathbf{b}}=\mathcal{B}\vec{\mathbf{b}}-\vec{\mathbf{c}}, \tag{33}$$

where $b_k=\langle\hat{\mathbf{B}}_k\rangle$. Equation (32) can describe the dynamics of a very general cycle of operation where the working medium is in contact with a heat bath and a variable external field. A particular example is chosen for analysis.

B. Integrating the equations of motion for the Otto cycle

The thermodynamical observables require the solution of the equations of motion on the two *isochores* and two *adiabats*. On the *isochores*, the field values ω are constant thus allowing a closed form solution. On the *adiabats*, ω changes with time and the coupling constants to the heat baths are zero. Therefore, solving the equation of motion either requires a numerical solution or finding a particular solution based on an explicit time dependence of ω.

Solving the equations of motion on the isochores

On the *isochores*, the coefficients in Eq. (33) are time independent. A solution is found by diagonalizing the $\mathcal{B}$ matrix leading to the eigenvalues: $-\Gamma-i\sqrt{2}\Omega-2\gamma\Omega^2$, $-\Gamma$, and $-\Gamma+i\sqrt{2}\Omega-2\gamma\Omega^2$. The diagonalization enables us to perform in closed form the exponentiation of $e^{\mathcal{B}'\Delta t}$ obtaining the propagator of the working medium operators $\mathcal{U}(\Delta t)$:

$$\mathcal{U}(\Delta t)=\mathcal{R}\begin{pmatrix} e^{-(\Gamma+i\sqrt{2}\Omega+2\gamma\Omega^2)\Delta t} & 0 & 0\\ 0 & e^{(-\Gamma\Delta t)} & 0\\ 0 & 0 & e^{-(\Gamma-i\sqrt{2}\Omega+2\gamma\Omega^2)\Delta t}\end{pmatrix}\mathcal{R}^{-1},$$

where

$$\mathcal{R}=\begin{pmatrix} iJ/\sqrt{2}\Omega & \omega/\Omega & -iJ/\sqrt{2}\Omega\\ -i\omega/\sqrt{2}\Omega & J/\Omega & i\omega/\sqrt{2}\Omega\\ 1/\sqrt{2} & 0 & 1/\sqrt{2}\end{pmatrix}, \tag{34}$$

leading to the final result

$$\mathcal{U}(\Delta t)=\exp[-(\Gamma+2\gamma\Omega^2)\Delta t]\begin{pmatrix} \frac{X\omega^2+cJ^2}{\Omega^2} & \frac{\omega J(X-c)}{\Omega^2} & \frac{Js}{\Omega}\\ \frac{\omega J(X-c)}{\Omega^2} & \frac{XJ^2+c\omega^2}{\Omega^2} & \frac{-\omega s}{\Omega}\\ -\frac{Js}{\Omega} & \frac{\omega s}{\Omega} & c\end{pmatrix}, \tag{35}$$

where $X=\exp(2\gamma\Omega^2\Delta t)$, $c=\cos(\sqrt{2}\Omega\Delta t)$, and $s=\sin(\sqrt{2}\Omega\Delta t)$. The solution of Eq. (32) then becomes

$$\vec{\mathbf{b}}(t+\Delta t)=\mathcal{U}(\Delta t)(\vec{\mathbf{b}}(t)-\vec{\mathbf{b}}^{\mathbf{eq}})+\vec{\mathbf{b}}^{\mathbf{eq}}, \tag{36}$$

where the equilibrium values of the operators are calculated from the steady state solutions of Eq. (33):

$$b_1^{eq}=\langle\hat{\mathbf{B}}_{\mathbf{1}}^{\mathbf{eq}}\rangle=-\frac{\sqrt{2}\omega}{\Omega Z}\sinh(\Omega\beta/\sqrt{2})=-\frac{\omega}{\sqrt{2}\Omega}\frac{k_\downarrow-k_\uparrow}{\Gamma},$$

$$b_2^{eq}=\langle\hat{\mathbf{B}}_{\mathbf{2}}^{\mathbf{eq}}\rangle=-\frac{\sqrt{2}\mathrm{J}}{\Omega Z}\sinh(\Omega\beta/\sqrt{2})=-\frac{\mathrm{J}}{\sqrt{2}\Omega}\frac{k_\downarrow-k_\uparrow}{\Gamma}, \tag{37}$$

$$b_3^{eq}=\langle\hat{\mathbf{B}}_{\mathbf{3}}^{\mathbf{eq}}\rangle=0.$$

On the *isochores*, the solution of Eq. (35) can be extended to the full duration $\tau_{h/c}$ of propagation on the hot (cold) branches. Therefore, $\Delta t=\tau_{h/c}$.

There are cycles of operation where the external field ω also varies when the working medium is in contact with the hot or cold baths, for example, the Carnot cycle [11]. For such cycles, the equation of motion can be solved by decomposing these branches into small segments of duration Δt. Then, Eq. (36) can be used as an approximate to the short time propagator.

C. Propagation of the observables on the adiabats

The equations of motion on the *adiabats* have explicit time dependence. To overcome this difficulty, two approaches are followed. The first is based on decomposing the evolution to short time segments and using a short time approximation to solve the equations of motion. The second approach is based on finding a particular time dependence form of $\omega(t)$, which allows an analytic solution.

1. Short time approximation

For the *adiabatic* branches, the working medium is decoupled from the baths so that the time propagation is unitary. Equation (32) thus simplifies to

$$\frac{d}{dt}\begin{pmatrix}b_1\\b_2\\b_3\end{pmatrix}=\begin{pmatrix}0&0&\sqrt{2}J\\0&0&-\sqrt{2}\omega(t)\\-\sqrt{2}J&\sqrt{2}\omega(t)&0\end{pmatrix}\begin{pmatrix}b_1\\b_2\\b_3\end{pmatrix}, \tag{38}$$

or in the vector form $(d/dt)\vec{\mathbf{b}}=\tilde{L}(t)\vec{\mathbf{b}}$. Since the matrix $\tilde{L}(t)$ is time dependent, the propagation is broken into short time segments Δt, reflecting the fact that $[\tilde{L}(t),\tilde{L}(t')]\neq 0$,

$$\vec{\mathbf{b}}(t)=\prod_{j=1}^{N}\exp\left(\int_{(j-1)\Delta t}^{j\Delta t}\tilde{L}(t')dt'\right)\vec{\mathbf{b}}(0), \tag{39}$$

where $N\Delta t=t$. Equation (38) is solved by diagonalizing the matrix $\tilde{L}$ for each time step assuming that during the period Δt, $\omega(t)$ is constant. Under such conditions, $\mathcal{U}_a(t,\Delta t)$ becomes (the index a stands for *adiabat*)

$$\mathcal{U}_a(t,\Delta t)=e^{\tilde{L}(t)\Delta t}=\begin{pmatrix}\frac{\omega^2+cJ^2}{\Omega^2}&\frac{\omega J(1-c)}{\Omega^2}&\frac{Js}{\Omega}\\\frac{\omega J(1-c)}{\Omega^2}&\frac{J^2+c\omega^2}{\Omega^2}&-\frac{\omega s}{\Omega}\\-\frac{Js}{\Omega}&\frac{\omega s}{\Omega}&c\end{pmatrix}, \tag{40}$$

which becomes the short time propagator for the adiabats from time t to $t+\Delta t$.

2. An analytical solution on the adiabats

The analytic solution for the propagator on the *adiabats* is based on the Lie group structure of the $\{\hat{\mathbf{B}}\}$ operators. The solution is based on the unitary evolution operator $\hat{\mathbf{U}}(t)$, which for explicitly time dependent Hamiltonians is obtained from the Schrödinger equation:

$$-i\frac{d}{dt}\hat{\mathbf{U}}(t)=\hat{\mathbf{H}}(t)\hat{\mathbf{U}}(t),\quad \hat{\mathbf{U}}(0)=\hat{\mathbf{I}}. \tag{41}$$

The propagated set of operators becomes

$$\vec{\hat{\mathbf{B}}}(t)=\hat{\mathbf{U}}(t)\vec{\hat{\mathbf{B}}}(0)\hat{\mathbf{U}}^{\dagger}(t)=\mathcal{U}_a(t)\vec{\hat{\mathbf{B}}}(0), \tag{42}$$

and is related to the superevolution operator $\mathcal{U}_a(t)$. Based on the group structure, Wei and Norman [37] constructed a solution to Eq. (41) for any operator $\hat{\mathbf{H}}$, which can be written as a linear combination of the operators in the closed Lie algebra $\hat{\mathbf{H}}(t)=\sum_{j=1}^{m}h_j(t)\hat{\mathbf{B}}_{\mathbf{i}}$, where the $h_i(t)$ are scalar functions of t, [cf. Eq. (10)]. In such a case, the unitary evolution operator $\hat{\mathbf{U}}(t)$ can be represented in the product form:

$$\hat{\mathbf{U}}(t)=\prod_{k=1}^{m}\exp[\alpha_k(t)\hat{\mathbf{B}}_k]. \tag{43}$$

The product form replaces the time dependent operator equation (38) with a set of scalar differential equations for the functions $\alpha_k(t)$. As has been shown in Sec. III A 2, three $\hat{\mathbf{B}}_{\mathbf{k}}$ operators form a closed Lie algebra. Writing the unitary evolution operator explicitly leads to

$$\hat{\mathbf{U}}(t)=\exp\left[i\frac{\alpha_1(t)}{\sqrt{2}}\hat{\mathbf{B}}_{\mathbf{1}}\right]\exp\left[i\frac{\alpha_2(t)}{\sqrt{2}}\hat{\mathbf{B}}_{\mathbf{2}}\right]\exp\left[i\frac{\alpha_3(t)}{\sqrt{2}}\hat{\mathbf{B}}_{\mathbf{3}}\right]. \tag{44}$$

The $\sqrt{2}$ factor is introduced for technical reasons. Based on the group structure [37], Eq. (41) leads to the following set of differential equations has to be solved:

$$\dot{\alpha}_1=\sqrt{2}\omega(t)+\sqrt{2}J\left[\frac{\sin(\alpha_1)\sin(\alpha_2)}{\cos(\alpha_2)}\right];$$

$$\dot{\alpha}_2=\sqrt{2}J\cos(\alpha_1);\quad \dot{\alpha}_3=\frac{\sqrt{2}J\sin(\alpha_1)}{\cos(\alpha_2)}. \tag{45}$$

Using Eq. (42), the propagator $\mathcal{U}_a(t)$ is evaluated explicitly in terms of the coefficients α:

$$\mathcal{U}_a(t)=\begin{pmatrix} c_2c_3 & -s_3c_1+c_3s_2s_1 & c_3s_2c_1+s_3s_1 \\ c_2s_3 & c_3c_1+s_3s_2s_1 & s_3s_2c_1-c_3s_1 \\ -s_2 & c_2s_1 & c_2c_1 \end{pmatrix}, \tag{46}$$

where $s_1=\sin(\alpha_1)$, $s_2=\sin(\alpha_2)$, $s_3=\sin(\alpha_3)$, $c_1=\cos(\alpha_1)$, $c_2=\cos(\alpha_2)$, and $c_3=\cos(\alpha_3)$.

The problem of obtaining a closed form solution for the propagator $\mathcal{U}_a(t)$ has been transformed into finding the solution of three coupled differential equations, Eq. (45), which depend on $\omega(t)$. A general solution has not been found, but by choosing a particular functional form for $\omega(t)$, a closed form solution has been obtained.

3. The explicit solution for α

To facilitate the solution of Eq. (45), a particular form of $\omega(t)$ is chosen:

$$\omega(t)=\frac{\dot{\alpha}_1}{\sqrt{2}}-J\frac{\sin(\alpha_1)\sin(\alpha_2)}{\cos(\alpha_2)}. \tag{47}$$

Two auxiliary functions are defined, $u(t)$ and $v(t)$:

$$u(t)=-J^2t^2+\sqrt{2}rJt;\quad v(t)=r-\sqrt{2}Jt. \tag{48}$$

Here, r is a constant which restricts the product Jt: $\{0<r<1;\ Jt<\sqrt{2}r\}$. In terms of $u(t)$ and $v(t)$, the solutions of Eq. (45) become

$$\alpha_1=\arccos\left(\frac{1}{\sqrt{1+2u}}\right), \tag{49}$$

$$\alpha_2=\arcsin\left(\frac{1}{1+r^2}(r\sqrt{1+2u}-v)\right), \tag{50}$$

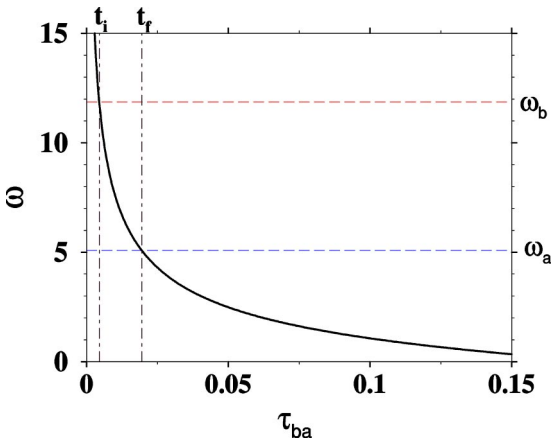

FIG. 2. The external field ω as a function of time on the *adiabats* corresponding to the function, Eq. (52), for which an analytic solution exists. Indicated are the values of the initial and the final time and of the corresponding ω, which are used to construct the cycle of operation. Note the singularity at $t=0$.

$$\begin{aligned}\alpha_3=&-\frac{r}{2}\ln(2\sqrt{4u^2+2u}+4u+1)\\&-\frac{\sqrt{1-r^2}}{2}\left\{\arcsin\left[\frac{2r^2(1-r^2)}{2u+1-r^2}+1-2r^2\right]-\frac{\pi}{2}\right\}\\&-\left\{\arcsin\left[\frac{v}{r}\right]-\frac{\pi}{2}\right\}-\frac{\sqrt{1-r^2}}{2}\left\{\arcsin\left[\frac{1}{r}\left[1-\frac{1-r^2}{1+v}\right]\right]\right.\\&\left.+\arcsin\left(\frac{1}{r}\left[1-\frac{1-r^2}{1-v}\right]\right)\right\}.\end{aligned} \tag{51}$$

For $t=0$, $\hat{\mathbf{U}}=\hat{\mathbf{I}}$, therefore $\alpha_1(0)=0$, $\alpha_2(0)=0$, $\alpha_3(0)=0$, which is consistent with Eqs. (49),(50), and (51).

Substituting into Eqs. (47), the explicit functional forms of α_k, $\omega(t)$ becomes

$$\omega(t)=\frac{Jv}{\sqrt{2}(1+2u)\sqrt{u}}-J\frac{\sqrt{2}\sqrt{u}(r\sqrt{1+2u}-v)}{\sqrt{1+2u}(\sqrt{1+2u}+rv)}. \tag{52}$$

At $t=0$, ω is singular. Since the engine operates between two finite values of ω, a corresponding time segment is chosen which does not include the singularity at $t=0$ (cf. Fig. 2). Using the group property of $\mathcal{U}_a(t)$, i.e., $\mathcal{U}_a(t_1)\mathcal{U}_a(t_2)=\mathcal{U}_a(t_1+t_2)$, the propagation is carried out by changing the origin of time, $\mathcal{U}_a(t)=\mathcal{U}_a^{-1}(t_0)\mathcal{U}_a(t+t_0)$ where t_0 is either t_i for the compression *adiabat* or t_f for the expansion *adiabat*. One should note that $\mathcal{U}_a^{-1}(t)=\mathcal{U}_a^{\dagger}(t)$, but due to the explicit time dependence $\mathcal{U}_a^{-1}(t)\neq\mathcal{U}_a^{\dagger}(-t)$.

IV. RECONSTRUCTION OF $\hat{\rho}^R$ (SCHRÖDINGER PICTURE)

The reconstruction of $\hat{\boldsymbol{\rho}}$, Eq. (7), is designed to describe the state of the working medium from its initial state to equi-

librium. As was analyzed in the preceding section, the set of operators $\hat{\mathbf{B}}_1, \hat{\mathbf{B}}_2, \hat{\mathbf{B}}_3, \hat{\mathbf{I}}$ is sufficient to describe the energy changes during the cycle of operation of the engine. Is this set sufficient to reconstruct the density operator?

In equilibrium, $\hat{\boldsymbol{\rho}}^{eq}$ is diagonal in the energy representation. From the eigenvalues of the Hamiltonian, Eq. (28), $\hat{\boldsymbol{\rho}}^{eq}$ in the energy picture becomes

$$\hat{\rho}_e^{eq} = \begin{pmatrix} \frac{e^{\Omega\beta/\sqrt{2}}}{Z} & 0 & 0 & 0 \\ 0 & \frac{1}{Z} & 0 & 0 \\ 0 & 0 & \frac{1}{Z} & 0 \\ 0 & 0 & 0 & \frac{e^{-\Omega\beta/\sqrt{2}}}{Z} \end{pmatrix}, \tag{53}$$

where

$$\begin{aligned} Z &= \exp-(\Omega\beta/\sqrt{2}) + 2 + \exp(\Omega\beta/\sqrt{2}) \\ &= \frac{k_\uparrow}{k_\downarrow} + 2 + \frac{k_\downarrow}{k_\uparrow} = \frac{\Gamma^2}{k_\downarrow k_\uparrow}. \end{aligned} \tag{54}$$

By inspection, the diagonal elements of the equilibrium density operator are seen to be defined by three independent variables. The energy expectation accounts for one variable. The expectation value of $\hat{\mathbf{B}}_3$ has no diagonal elements in the energy representation, therefore two additional operators are required to facilitate a reproduction of $\hat{\boldsymbol{\rho}}^R$:

$$\hat{\mathbf{B}}_4 = 2^{-3/2}(\hat{\boldsymbol{\sigma}}_z^1 \otimes \hat{\mathbf{I}}^2 - \hat{\mathbf{I}}^1 \otimes \hat{\boldsymbol{\sigma}}_z^2) = \frac{1}{\sqrt{2}} \begin{pmatrix} 0 & 0 & 0 & 0 \\ 0 & 1 & 0 & 0 \\ 0 & 0 & -1 & 0 \\ 0 & 0 & 0 & 0 \end{pmatrix}, \tag{55}$$

and

$$\hat{\mathbf{B}}_5 = \frac{1}{2}\hat{\boldsymbol{\sigma}}_z^1 \otimes \hat{\boldsymbol{\sigma}}_z^2 = \frac{1}{2} \begin{pmatrix} 1 & 0 & 0 & 0 \\ 0 & -1 & 0 & 0 \\ 0 & 0 & -1 & 0 \\ 0 & 0 & 0 & 1 \end{pmatrix}. \tag{56}$$

Since both $\hat{\mathbf{B}}_4$ and $\hat{\mathbf{B}}_5$ commute with the Hamiltonian, these undergo only dissipative dynamics but these are uninfluenced by the dephasing generated by $\mathcal{L}_D^*$:

$$\dot{\hat{\mathbf{B}}}_4 = -\Gamma \hat{\mathbf{B}}_4 \tag{57}$$

with the solution

$$\hat{\mathbf{B}}_4(t) = \hat{\mathbf{B}}_4(0)\exp(-\Gamma t), \tag{58}$$

and $\langle \hat{\mathbf{B}}_4^{\mathbf{eq}} \rangle = 0$. The equation of motion of $\hat{\mathbf{B}}_5$ is

$$\begin{aligned} \dot{\hat{\mathbf{B}}}_5 &= -2\Gamma \hat{\mathbf{B}}_5 - \sqrt{2}\,\frac{\omega}{\Omega}(k_\downarrow - k_\uparrow)\hat{\mathbf{B}}_1 - \sqrt{2}\,\frac{\mathrm{J}}{\Omega}(k_\downarrow - k_\uparrow)\hat{\mathbf{B}}_2 \\ &= -2\Gamma \hat{\mathbf{B}}_5 + 2\Gamma \langle \hat{\mathbf{B}}_1^{\mathbf{eq}} \rangle \hat{\mathbf{B}}_1 + 2\Gamma \langle \hat{\mathbf{B}}_2^{\mathbf{eq}} \rangle \hat{\mathbf{B}}_2. \end{aligned} \tag{59}$$

At equilibrium, $\dot{\hat{\mathbf{B}}}_5 = 0$, and then $\langle \hat{\mathbf{B}}_5^{\mathbf{eq}} \rangle = (\hat{\mathbf{B}}_1^{\mathbf{eq}})^2 + (\hat{\mathbf{B}}_2^{\mathbf{eq}})^2$, a result which can be verified by computing $\langle \hat{\mathbf{B}}_5^{\mathbf{eq}} \rangle = \mathrm{tr}\{\hat{\boldsymbol{\rho}}^{\mathbf{eq}} \hat{\mathbf{B}}_5\}$. Equation (59) is a linear first-order inhomogeneous equation for $\hat{\mathbf{B}}_5$ depending on the time dependence of the closed set $\hat{\mathbf{B}}_1, \hat{\mathbf{B}}_2, \hat{\mathbf{B}}_3$, Eq. (36). Changing Eq. (59) to observables, Eq. (1), and by integrating subject to the solutions of b_1 and b_2 leads to

$$\begin{aligned} b_5(t) = \frac{2}{\Omega^2}\{&\omega[b_1(0) - b_1^{eq}] + J[b_2(0) - b_2^{eq}]\} \\ &\times (\omega b_1^{eq} + J\ b_2^{eq})(e^{-\Gamma t} - e^{-2\Gamma t}) \\ &+ k_0[k_1 c(e^{-(\Gamma + 2\gamma\Omega^2)t}) + k_2\ se^{-(\Gamma + 2\gamma\Omega^2)t} \\ &- k_1 e^{-2\Gamma t}] + [b_5(0) - b_5^{eq}]e^{-2\Gamma t} + b_5^{eq}, \end{aligned} \tag{60}$$

where

$$k_0 = \frac{2\Gamma(Jb_1^{eq} - \omega b_2^{eq})}{\Omega^2[(\Gamma - 2\gamma\Omega^2)^2 + 2\Omega^2]}, \tag{61}$$

$$\begin{aligned} k_1 = \{&J[b_1(0) - b_1^{eq}] - \omega[b_2(0) - b_2^{eq}]\}(\Gamma + 2\gamma\Omega^2) \\ &- \Omega[b_3(0) - b_3^{eq}](\sqrt{2}\Omega), \end{aligned}$$

and

$$\begin{aligned} k_2 = \{&J[b_1(0) - b_1^{eq}] - \omega[b_2(0) - b_2^{eq}]\}(\sqrt{2}\Omega) \\ &+ \Omega[b_3(0) - b_3^{eq}](\Gamma - 2\gamma\Omega^2). \end{aligned}$$

Using the set of the five orthogonal and normalized operators together with the identity operator, the density operator $\hat{\boldsymbol{\rho}}^R$ is reconstructed. Representing $\hat{\boldsymbol{\rho}}_R$ in different bases facilitates the calculation of the different entropies. $\hat{\boldsymbol{\rho}}_R$ in the polarization basis becomes

$$\hat{\boldsymbol{\rho}}_p = \begin{pmatrix} \frac{1}{4}+\frac{b_1}{\sqrt{2}}+\frac{b_5}{2} & 0 & 0 & \frac{b_2}{\sqrt{2}}-i\frac{b_3}{\sqrt{2}} \\ 0 & \frac{1}{4}+\frac{b_4}{\sqrt{2}}-\frac{b_5}{2} & 0 & 0 \\ 0 & 0 & \frac{1}{4}-\frac{b_4}{\sqrt{2}}-\frac{b_5}{2} & 0 \\ \frac{b_2}{\sqrt{2}}+i\frac{b_3}{\sqrt{2}} & 0 & 0 & \frac{1}{4}-\frac{b_1}{\sqrt{2}}+\frac{b_5}{2} \end{pmatrix}. \tag{62}$$

The off-diagonal elements of $\hat{\boldsymbol{\rho}}_p$ are the expectation values of the operators $\hat{\mathbf{B}}_{\pm}=1/\sqrt{2}(\hat{\mathbf{B}}_2 \pm i\hat{\mathbf{B}}_3)$, which represent the correlation between the individual spins and also determine the entanglement.

The density operator $\hat{\boldsymbol{\rho}}^R$ in the energy basis becomes

$$\hat{\boldsymbol{\rho}}_e = \begin{pmatrix} \frac{1}{4}-\frac{E}{\Omega\sqrt{2}}+\frac{b_5}{2} & 0 & 0 & +\frac{ib_3}{\sqrt{2}}-\frac{Jb_1}{\Omega\sqrt{2}}+\frac{\omega b_2}{\Omega\sqrt{2}} \\ 0 & \frac{1}{4}+\frac{b_4}{\sqrt{2}}-\frac{b_5}{2} & 0 & 0 \\ 0 & 0 & \frac{1}{4}-\frac{b_4}{\sqrt{2}}-\frac{b_5}{2} & 0 \\ -\frac{ib_3}{\sqrt{2}}-\frac{Jb_1}{\Omega\sqrt{2}}+\frac{\omega b_2}{\Omega\sqrt{2}} & 0 & 0 & \frac{1}{4}+\frac{E}{\Omega\sqrt{2}}+\frac{b_5}{2} \end{pmatrix}, \tag{63}$$

where $E=\omega b_1+Jb_2$. In equilibrium, the off-diagonal elements vanish, and the matrix will be identical to Eq. (53). In nonequilibrium, the off-diagonal elements of $\hat{\boldsymbol{\rho}}_e$ determine the ''phase,'' cf. Sec. VII.

To compute the von Neumann entropy, $\hat{\boldsymbol{\rho}}^R$ is diagonalized leading to

$$\hat{\rho}_{vn} = \begin{pmatrix} \frac{1}{4}-\frac{D}{\sqrt{2}}+\frac{b_5}{2} & 0 & 0 & 0 \\ 0 & \frac{1}{4}+\frac{b_4}{\sqrt{2}}-\frac{b_5}{2} & 0 & 0 \\ 0 & 0 & \frac{1}{4}-\frac{b_4}{\sqrt{2}}-\frac{b_5}{2} & 0 \\ 0 & 0 & 0 & \frac{1}{4}+\frac{D}{\sqrt{2}}+\frac{b_5}{2} \end{pmatrix}, \tag{64}$$

where $D=\sqrt{b_1^2+b_2^2+b_3^2}$.

V. THE THERMODYNAMIC QUANTITIES FOR THE COUPLED SPIN FLUID

The solution of the equation of motion for the expectation values and the reconstruction of the state $\hat{\boldsymbol{\rho}}^R$ are the prerequisite for calculating the thermodynamical observables on all branches of the engine. The explicit equations for these quantities are now derived.

A. Dynamical temperature (T_{dyn}) on the branches

Based on the definition of the dynamical temperature T_{dyn} in Eq. (21), and from Eq. (27),

$$T_{dyn}=\frac{\dot{\omega}b_1+\omega\dot{b}_1+J\dot{b}_2}{-\sum \dot{p}_i^E[1+\ln(p_i^E)]}$$

$$=\frac{\dot{\omega}b_1-\Gamma E-\frac{\Omega}{\sqrt{2}}(k_\downarrow-k_\uparrow)}{-\sum \dot{p}_i^E[1+\ln(p_i^E)]}, \quad (65)$$

The four probabilities p_i^E are the diagonal elements of the density operator in the energy representation $\hat{\boldsymbol{\rho}}_e$, Eq. (63). The derivatives of the probabilities are obtained from Eqs. (32) and (59):

$$\dot{p}_1^E=\frac{-\dot{\omega}b_1+\Gamma E}{\Omega\sqrt{2}}+\frac{(k_\downarrow-k_\uparrow)}{2}+\frac{\dot{b}_5}{2}, \quad \dot{p}_2^E=-\frac{\dot{b}_5}{2},$$

$$\dot{p}_3^E=-\frac{\dot{b}_5}{2}, \quad \dot{p}_4^E=\frac{\dot{\omega}b_1-\Gamma E}{\Omega\sqrt{2}}-\frac{(k_\downarrow-k_\uparrow)}{2}+\frac{\dot{b}_5}{2}, \quad (66)$$

where $\dot{b}_5$ is obtained from Eq. (59), $\dot{b}_5=2\Gamma(b_1^{eq}b_1+b_2^{eq}b_2-b_5)$.

1. Dynamical temperature on the isochores

Evaluating the derivatives of the probabilities in Eqs. (66) and using the fact that on the *isochores* $\dot{\omega}=0$, the dynamical temperature, Eq. (65), becomes

$$T_{dyn}=\frac{\left[\Gamma E+\frac{\Omega}{\sqrt{2}}(k_\downarrow-k_\uparrow)\right]}{\left[\frac{\Gamma E}{\Omega\sqrt{2}}\ln(p_1/p_4)+\frac{(k_\downarrow-k_\uparrow)}{2}\ln(p_1/p_4)+\frac{1}{2}\dot{b}_5\ln(p_1p_4/p_2p_3)\right]}. \quad (67)$$

A consistency check is obtained by comparing T_{dyn} for $J=0$ with the internal temperature of a two-level system. For $J=0$,

$$T_{dyn}=\frac{\omega}{\sqrt{2}\ln\left(\frac{1/2+b_1/\sqrt{2}}{1/2-b_1/\sqrt{2}}\right)}, \quad (68)$$

which leads to

$$b_1=-1/\sqrt{2}\,\frac{k_\downarrow-k_\uparrow}{k_\downarrow+k_\uparrow}=-1/\sqrt{2}\tanh\left(\frac{\omega}{\sqrt{2}T_{dyn}}\right), \quad (69)$$

which is the internal temperature for a noninteracting spin system with energy spacing $\omega/\sqrt{2}$ [10].

2. Dynamical temperature on the adiabats

On the *adiabats* $\dot{b}_4=$ and $\dot{b}_5=0$. From Eqs. (65) and (66), the derivatives of the probabilities on the adiabats become for constant Ω,

$$\dot{p}_1^E=-\frac{\dot{\omega}}{\Omega\sqrt{2}}; \quad \dot{p}_2^E=0; \quad \dot{p}_3^E=0; \quad \dot{p}_4^E=\frac{\dot{\omega}}{\Omega\sqrt{2}}, \quad (70)$$

leading to the dynamical temperature on the *adiabats*:

$$T_{dyn}^{ad}=\frac{\Omega\sqrt{2}}{\ln\left(\frac{p_1^E}{p_4^E}\right)}, \quad (71)$$

which could be obtained directly from the density operator in the energy representation, Eq. (63).

B. The heat absorbed or delivered by the heat engine

Using Eq. (15), the heat $\mathcal{Q}_{\mathrm{h/c}}$ absorbed or delivered on the *isochores* becomes

$$\mathcal{Q}_{\mathrm{i}}=[\exp(-\Gamma\tau_i)-1](\omega_i b_1+Jb_2), \quad (72)$$

where $i=h/c$.

C. The work absorbed or delivered by the heat engine

The power absorbed or emitted on the *adiabats*, cf. Eq. (14), becomes

$$\mathcal{P}=\left\langle\frac{\partial H}{\partial t}\right\rangle=\dot{\omega}\langle\hat{\mathbf{B}}_1\rangle. \quad (73)$$

In the limit of slow change of ω, the state of the system follows adiabatically the Hamiltonian. This means that the diagonal elements of the state in the energy representation $\hat{\boldsymbol{\rho}}_e$, Eq. (63), do not change. Stated differently, $\langle\hat{\mathbf{H}}\rangle/\Omega$ is a constant. In this limit, the power becomes

$$\mathcal{P}_{slow}=\dot{\Omega}\frac{\langle\hat{\mathbf{H}}\rangle}{\Omega}. \quad (74)$$

Equation (74) suggests a decomposition of the power, Eq. (73), into a component in the energy direction and a perpendicular contribution leading to

$$\mathcal{P}=\dot{\Omega}\frac{\langle\hat{\mathbf{H}}\rangle}{\Omega}+\frac{\dot{\omega}J}{\Omega^2}(J\langle\hat{\mathbf{B}}_1\rangle-\omega\langle\hat{\mathbf{B}}_2\rangle), \tag{75}$$

where the first term, which is diagonal in the energy frame, represents the power required to change the field against the response of the system. The second term is the additional power required to drive the working fluid in a finite rate. This term is interpreted as the power invested against friction and it vanishes when $J=0$ or $\dot{\omega}=0$. The additional power comes from the off-diagonal elements in the energy representation. The total work on the *adiabatic* branches is obtained by integrating the power:

$$\mathcal{W}=\int_{\tau i}^{\tau \mathbf{f}} b_1\dot{\omega}dt, \tag{76}$$

which leads to the slow limit $\mathcal{W}_{slow}=(\Omega_f-\Omega_i)E(t)/\Omega$.

D. Entropy production

Since the engine operation is cyclic, entropy production, $\mathcal{D}S_{cycle}$, is created on the boundaries with the heat bath [cf. Eq. (17)] i.e., on the *isochores*:

$$\mathcal{D}S_{cycle}=-(\mathcal{Q}_{\mathrm{AB}}/T_h+\mathcal{Q}\mathrm{CD}/T_c). \tag{77}$$

E. Efficiency

The efficiency per cycle, η_{cycle}, is

$$\eta_{cycle}=\mathcal{W}/\mathcal{Q}_{\mathrm{AB}}=\frac{\int_{\tau i}^{\tau \mathbf{f}} b_1\dot{\omega}dt}{[\exp(-\Gamma\tau_{\mathrm{i}})-1](\omega_{\mathrm{i}}b_1+Jb_2)}. \tag{78}$$

The maximal efficiency of the engine is

$$\eta_{max}=1-\frac{\Omega_a}{\Omega_b}=1-\frac{\sqrt{\omega_a^2+J^2}}{\sqrt{\omega_b^2+J^2}},$$

which is below the Carnot efficiency, for all J since the engine produces power only when $\omega_a/\omega_b>T_c/T_h$:

$$\eta_{max}=1-\frac{\sqrt{\omega_a^2+J^2}}{\sqrt{\omega_b^2+J^2}}<1-\frac{\omega_a}{\omega_b}<1-\frac{T_c}{T_h}. \tag{79}$$

VI. THE CYCLE OF OPERATION: THE OTTO CYCLE

The operation of the heat engine is determined by the properties of the working medium and by the hot and cold baths. These properties are summarized by the generator of the dynamics $\mathcal{L}$. The cycle of operation is defined by the external controls that include the variation in time of the field with the periodic property $\omega(t)=\omega(t+\tau)$, where τ is the total cycle time synchronized with the contact times of the working medium with the hot and cold baths τ_h and τ_c. In this study, a specific operating cycle composed of two branches termed *isochores*, where the field is kept constant and the working medium is in contact with the hot (cold) baths. In addition, two branches termed *adiabats* where the field $\omega(t)$ varies and the working medium is disconnected from the baths. This cycle is a quantum analog of the Otto cycle.

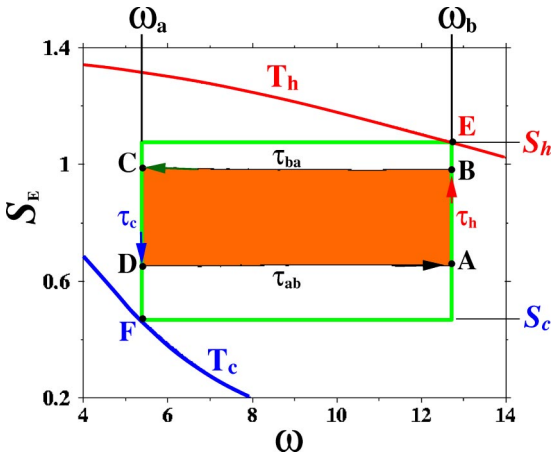

FIG. 3. The heat engine's optimal cycles in the $(\omega,\mathcal{S}_E)$ plane. The upper line, denoted by T_h, indicates the energy entropy of the working medium in the equilibrium with the hot bath at temperature T_h for different values of the field. The line below, denoted by T_c, indicates the energy entropy in the equilibrium with the cold bath at temperature T_c. The cycle touching the points **E** and **F** has an infinite time allocation on all branches. It reaches the equilibrium point with the hot bath (point **E**) and equilibrium point with the cold bath (point **F**). The inner cycle **ABCD** is the optimal cycle with the optimal time allocation on all branches, calculated numerically for a linear ω dependence on time $\tau_h=3.0108$, $\tau_{ba}=0.301$, $\tau_c=3.014$, and $\tau_{ch}=0.346$. The external parameters are $\omega_a=5.382$, $\omega_b=12.717$, $J=2$, $T_h=7.5$, $T_c=1.5$, $\Gamma_h=0.382$, and $\Gamma_c=0.342$, and $\gamma_h=\gamma_c=0$.

The dynamics of the working medium has been described in Sec. III. The parameters defining the cycle are (1) T_h and T_b, the hot and cold bath temperatures; (2) Γ_h and Γ_c, the hot and cold bath heat conductance parameters; (3) γ_h and γ_c, the hot and cold bath dephasing parameters; (4) J—the strength of the internal coupling.

The external control parameter defines the four strokes of the cycle (cf. Fig. 3):

(1) *Isochore* **A**→**B**: when the field is maintained constant, $\omega=\omega_b$, the working medium is in contact with the hot bath for a period of τ_h.

(2) *Adiabat* **B**→**C**: when the field changes linearly from ω_b to ω_a in a time period of τ_{ba}.

(3) *Isochore* **C**→**D**: when the field is maintained constant, $\omega=\omega_a$, the working medium is in contact with the cold bath for a period of τ_c.

(4) Adiabat **D**→**A**: when the field changes linearly from ω_a to ω_b in a time period of τ_{ab}.

The trajectory of the cycle in the field and the entropy plane $(\omega,\mathcal{S}_E)$ is shown in Fig. 3, employing a numerical propagation with a linear ω dependence on time.

A different perspective of the dynamics during the cycle of operation is shown in Fig. 3, displaying the cycle trajectory in the b_1,b_2,b_3 coordinates. The hypothetical cycle

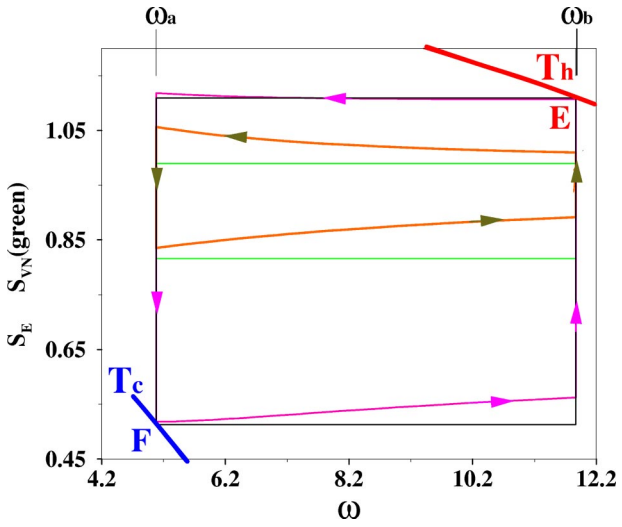

FIG. 4. Three cycles of operation based on the analytic solution in the $(\omega,\mathcal{S}_E)$ plane. The inner cycle, emphasized by arrows, has the shortest time allocations ($\tau_h=2$, $\tau_{ba}=\tau_{ab}=0.05$, $\tau_c=2.1$). The rectangle cycle shows the corresponding $(\omega,\mathcal{S}_{VN})$ plot. The outer cycle, emphasized by arrows, has longer time allocations $\tau_h=\tau_c=15$, $\tau_{ba}=\tau_{ab}=0.05$, while the black cycle has infinite time allocations on all branches, therefore, $\mathcal{S}_E=\mathcal{S}_{VN}$. This cycle touches the isothermal equilibrium points *E* and *F*. The common parameters for all the cycles are $J=2$, $r=0.96$, $T_h=7.5$, $T_c=1.5$, $\Gamma_h=\Gamma_c=0.3243$, $\gamma_h=\gamma_c=0$, $\omega_a=5.083\,64$, and $\omega_b=11.8675$.

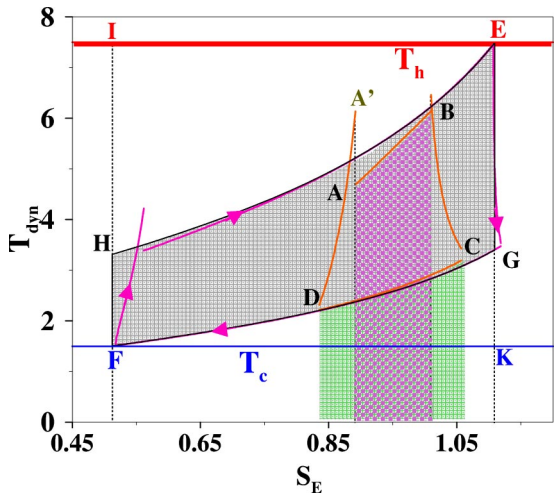

FIG. 5. The cycles in $(\mathcal{S}_E,T_{dyn})$ planes. The inner cycle **A,B,C,D** corresponds to the short time cycle of Fig. 4. The cycle indicated with arrows is the long time cycle and the cycle **H,E,G,F** corresponds to the cycle with infinite time allocation on all branches. The rectangle, including points **I,E,K,F,** is the work obtained in a Carnot cycle operating between T_h and T_c. The shaded area **H,E,G,F** represents the maximum work of the Otto cycle. The area below the **AB** segment is the heat transferred from the hot bath $\mathcal{Q}_h$. The area below the **DC** segment is the heat transferred to the cold bath $\mathcal{Q}_c$.

with infinitely long time on all branches would include the equilibrium points *E* and *F*. The cycle trajectory is planar on the $\hat{\mathbf{B}}_3=0$ plane as can be seen in panel *C*. The cycle *ABCD* with finite-time allocation spirals around the infinitely long time cycle with an incursion into the $\hat{\mathbf{B}}_3$ direction. The reference cycle with infinite time allocation on all branches is characterized by a diagonal state $\hat{\boldsymbol{\rho}}_e$ in the instantaneous energy representation. The slow motion on the *adiabats* allows the state $\hat{\boldsymbol{\rho}}$ to adopt to the changes in time of the Hamiltonian, which therefore can be termed adiabatic following. If the time allocation on the adiabats is short, nonadiabatic effects take place. In the sudden limit of infinite short time allocation on the *adiabat*, the state of the system has no time to evolve, $\hat{\boldsymbol{\rho}}(t_i+\tau_{ab})=\hat{\boldsymbol{\rho}}(t_i)$. Insight into the transition from the slow to the sudden limit is obtained by following the dynamics in the energy representation. In this time dependent frame the Liouville–von Neumann equation (2) becomes

$$\dot{\hat{\boldsymbol{\rho}}}_e=-i[\hat{\mathbf{H}}_e,\hat{\boldsymbol{\rho}}_e]+i\frac{\dot{\omega}J}{2\Omega^2}[\hat{\mathbf{B}}_3,\hat{\boldsymbol{\rho}}_e]. \tag{80}$$

The first term in the rhs of Eq. (80) generates a precession motion around the energy direction. If $\hat{\boldsymbol{\rho}}_e$ is diagonal, for example, when starting from thermal equilibrium, this term will vanish since it commutes with $\hat{\mathbf{H}}_e$. The second term generates a precession motion around the $\hat{\mathbf{B}}_3$ direction with a rate $\xi=\dot{\omega}J/\Omega^2$ leading to off-diagonal elements of $\hat{\boldsymbol{\rho}}_e$.

When following the direction of the cycle, the energy entropy increases on the *adiabats*. This is evident in Figs. 3 and 4. This entropy increase is the signature of nonadiabatic effects reflecting the inability of the population on the energy states to follow the change in time of the Hamiltonian. As a result, the energy dispersion increases. Since the evolution on these branches is unitary, $\mathcal{S}_{VN}$ is constant. When more time is allocated to the *adiabats*, the increase in $\mathcal{S}_E$ is smaller. For infinite time allocation, $\mathcal{S}_E=\mathcal{S}_{VN}$.

The larger curvature of the entropy increase in the analytic result of Fig. 4, compared with the numerical result of Fig. 3, reflects the difference in the dependence of $\omega(t)$ on time. When the analytic functional form of $\omega(t)$ is used in the numerical propagation, the numerical solution converges to the values of the analytic solution. This convergence test was used as a consistency check for both methods. This convergence was not uniform for all elements in the propagator [cf. Eqs. (40) and (46)]. Comparing the elements of the numerical propagator $\mathcal{U}_a(\tau_{ab})$ to the elements of analytic $\mathcal{U}_a(\tau_{ab})$, showed that the largest discrepancy between the individual elements at $t=\tau_{ab}$ was less than 10^{-3}, when a time step of $\Delta t=\tau_{ab}/1000$ was used.

In Fig. 5, the cycle of operation is presented in the energy-entropy internal-temperature coordinates $(\mathcal{S}_E,T_{dyn})$. The cycles shown correspond to the analytical cycles of Fig. 4. The discontinuities in the short time cycle reflect the overheating in the compression stage, shown as the difference between the points **A** and **A′** in Fig. 5. The heat accumulated is quenched when the working medium is put in contact with the hot bath. This phenomena has been identified in measurements of working fluid temperatures in actual heat engines or heat pumps [26]. A discontinuity as a result of the insufficient cooling of the working medium in the expansion

branch is also evident in the short time cycle. The magnitude of these discontinuities is reduced at longer times and disappears for the infinite long cycle where the working fluid reaches thermal equilibrium with the hot bath at point **E** and with the cold bath at point **F**. In this case, both *adiabatic* branches are isentropic. It is clear from Fig. 5 that for the cycles with vertical *adiabats*, the work is the area enclosed by the cycle trajectory. When the time allocation on the *adiabats* is restricted, this is no longer the case as due to the entropy increase, the area under the hot *isochore* does not cover the area under the cold *isochore*. Additional cooling is then required to dissipate the extra work required to drive the system on the *adiabats* at finite time.

VII. THE EFFECT OF PHASE AND DEPHASING

Performance of the heat engine explicitly depends on heat and work, which constitute the energy (16). Do other observables, incompatible with the energy, influence the engines performance? Examining the cycle trajectory on the *isochores* in Fig. 1, in addition to the motion in the energy direction, toward equilibration, spiraling motion exists. This motion is characterized by the amplitude and the phase of an observable in the plane perpendicular to the energy direction. The phase ϕ of this motion advances in time, i.e., $\phi \propto t$. The concept of phase has its origins in classical mechanics, where a canonical transformation leads to a new set of action angle variables. The conjugate variable to the Hamiltonian is the phase. In quantum mechanics, the phase observable has been a subject of continuous debate [38]. For a harmonic oscillator, it is related to the creation and anhilation operators $\hat{\mathbf{a}}$ [39,40]. In analogy the raising (lowering) operator is defined as

$$\hat{\mathbf{L}}_{\pm} = \frac{1}{\sqrt{2}\Omega}(-J\hat{\mathbf{B}}_1 + \omega\hat{\mathbf{B}}_2 \pm i\Omega\hat{\mathbf{B}}_3), \tag{81}$$

which has the following commutation relation with the Hamiltonian:

$$[\hat{\mathbf{H}}, \hat{\mathbf{L}}_{\pm}] = \pm\sqrt{2}\Omega\hat{\mathbf{L}}_{\pm}. \tag{82}$$

The free evolution of $\hat{\mathbf{L}}_{+}$ therefore becomes $\hat{\mathbf{L}}_{+}(t) = e^{i\sqrt{2}\Omega t}\hat{\mathbf{L}}_{+}(0)$, which defines the phase variable through $\langle\hat{\mathbf{L}}_{+}\rangle = re^{i\phi}$, therefore $\phi = \arctan[\Omega b_3/-Jb_1+\omega b_2]$. A corroboration for this interpretation is found by examining the state $\hat{\boldsymbol{\rho}}_e$ in the energy representation [cf. Eq. (63)]. The off-diagonal elements are completely specified by the expectation values of $\hat{\mathbf{L}}_{\pm}$.

The dynamics of $\hat{\mathbf{L}}_{\pm}$ on the *isochores* includes also dissipative contributions, which can be evaluated using Eq. (32):

$$\dot{\hat{\mathbf{L}}}_{\pm} = \pm i\sqrt{2}\Omega\hat{\mathbf{L}}_{\pm} - (\Gamma + 2\gamma\Omega^2)\hat{\mathbf{L}}_{\pm}. \tag{83}$$

Examining Eq. (83), it is clear that the amplitude of $\hat{\mathbf{L}}_{\pm}$ decays exponentially with the rate $1/T_2 = \Gamma + 2\gamma\Omega^2$, where Γ is the dephasing contribution due to energy relaxation and $1/T_2^* = 2\gamma\Omega^2$ is the pure dephasing contribution.

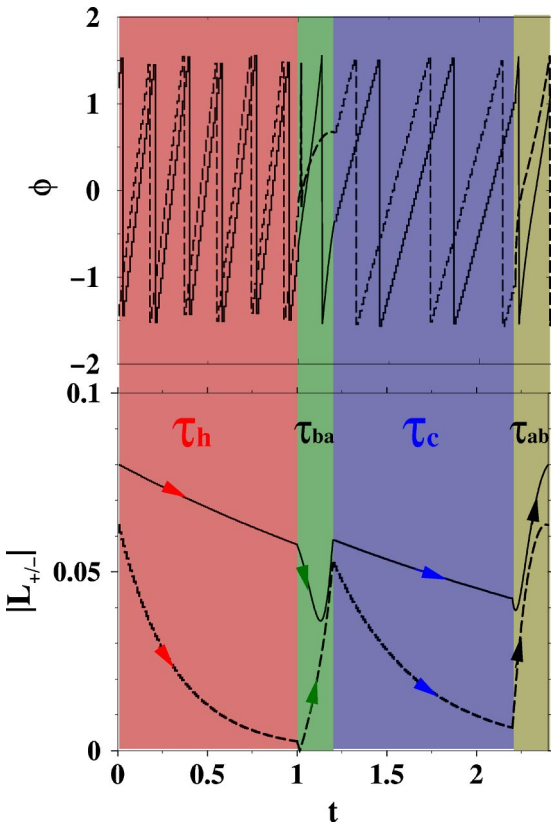

FIG. 6. The modulus and phase of $\hat{\mathbf{L}}_{\pm}$ as a function of time. The dashed lines include additional pure dephasing ($\gamma_h = 0.01, \gamma_c = 0.03$). The common parameters are $T_h = 7.5$, $T_c = 1.5$, $\Gamma_h = \Gamma_c = 0.34$, $\omega_b = 11.8675$ and $\omega_a = 5.083$, The total cycle time is $\tau = 2.4$, where $\tau_h = \tau_c = 1$, $\tau_{ba} = 0.2$, $\tau_{ab} = 0.2$.

Both Figs. 3 and 6 show that the dephasing is not complete at the end of the *isochores*. A small change in the time allocation in the order of $1/\Omega$ can completely change the final phase on the *isochore* and on the initial phase for the *adiabat*. This means that the cycle performance characteristic becomes very sensitive to small changes in time allocation on the *isochores*. This effect can be observed in Fig. 7 for the power and Fig. 8 for the entropy production. Examining Fig. 7 reveals that increasing J increases the "phase" effect. For $J = 2$, for specific time allocations, the power can even become negative. Increasing the dephasing rate either by adding pure dephasing or by changing the heat transfer rate reduces the "noise." This can also be seen in Fig. 8. An interesting phase effect can be observed in Fig. 9 where the cycle is displayed in the $(\mathcal{S}_E, T_{dyn})$ plane. The inner (solid black) cycle shows an energy-entropy decrease in the compression *adiabat*. The reason for this decrease is a phase memory from the compression *adiabat*, which is due to the insufficient dephasing on the cold *isochore*. Additional pure dephasing eliminates this entropy decrease as can be seen in the dashed black cycle. This cycle is also pushed to larger entropy values. The outer cycles are characterized by a longer time allocation on the *isochores*. For these cycles, the energy entropy always increases on the *adiabats*. This cycle is shifted by the dephasing to lower energy-entropy values.

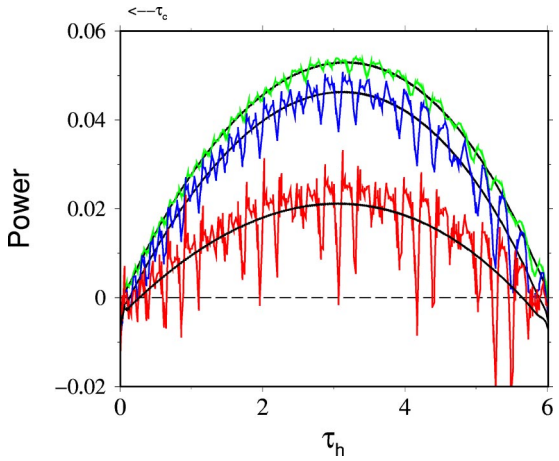

FIG. 7. The power produced by the engine as a function of the time allocation on the hot *isochore*. For the upper fluctuating curve, the cycle corresponds to J=1 and $\Gamma_h=\Gamma_c=0.324$. For the next from the top, corresponds to the cycle with $J=2$ and $\Gamma_h=\Gamma_c=0.324$. For the lower cycle corresponds to $J=24$ and $\Gamma_h=\Gamma_c=0.162$. The three fluctuating cycles have no pure dephasing $\gamma_h=\gamma_c=0$. With addition of dephasing $\gamma_h=0.01$ and $\gamma_c=0.03$, the noise is eliminated and the three cycles collapse to the solid lines. The common parameters are $T_h=7.5$, $T_c=1.5$, $\omega_b=12.717$, and $\omega_a=5.382$, The total cycle time τ is 6.74, $\tau_{ba}=0.3,\tau_{ab}=0.34$.

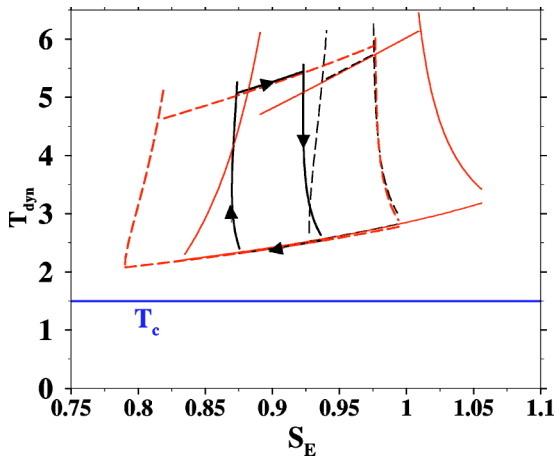

FIG. 9. The influence of dephasing on the cycle of operation in the $(\mathcal{S}_E, T_{dyn})$ plane. Solid curves correspond to an operation without pure dephasing. The dashed curves represent cycles including pure dephasing. For the inner cycles, the time allocations on the *isochores* are $\tau_h=\tau_c=0.6$. The pure dephasing parameter is $\gamma_h=\gamma_c=0$ for the solid lines, and $\gamma_h=0.005,\gamma_c=0.015$ for the dashed lines. For the outer cycles, the allocated times on the isochores are $\tau_h=2.,\tau_c=2.1$ with $\gamma_h=\gamma_c=0$ for the solid lines, and $\gamma_h=0.01,\gamma_c=0.03$ for the dashed lines. The common parameters for all four cycles are $J=2.$, $T_h=7.5$, $T_c=1.5$, $\Gamma_h=\Gamma_c=0.3243$, and $\tau_{ab}=\tau_{ba}=0.015$.

VIII. DISCUSSION

Quantum thermodynamics is the study of thermodynamical phenomena based on quantum mechanical principles [43]. To meet this challenge, quantum expectation values have to be related to thermodynamical variables. The Otto cycle is an *ab initio* quantum model for which analytic solutions have been obtained. The principle thermodynamical variables: energy entropy and temperature are derived from first principles. The solution of the quantum equations of motion for the state $\hat{\boldsymbol{\rho}}$ enables tracing the thermodynamical variables for each point on the cycle trajectory. This dynamical picture supplies a rigorous formalism for finite-time thermodynamics [21,24].

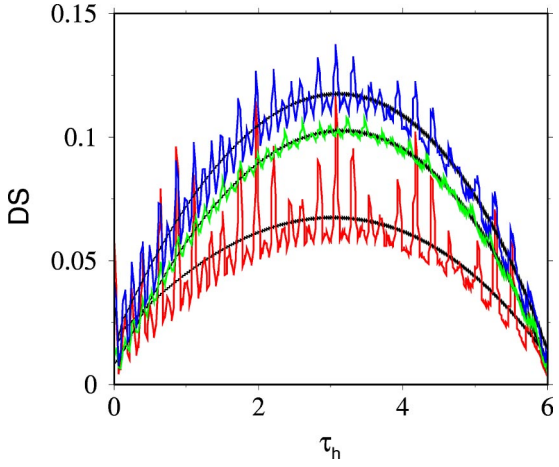

FIG. 8. Entropy productions $\mathcal{D}S_{cycle}$, Eq. (77), as a function of the time allocation on the hot *isochore*. The notations are the same as in Fig. 7.

An underlying principle of finite-time thermodynamics is that the operation irreversibilities are inevitable if a process runs at finite rate. Moreover, these irreversibilities are the source of performance limitations imposed on the process. The present Otto cycle heat engine in line with finite time thermodynamics (FTT) is subject to two major performance limitations:

(1) Finite rate of heat transfer from the hot bath to the working medium and from the working medium to the cold bath.

(2) Additional work invested in the expansion and compression branches is required to drive the *adiabats* at a finite time.

The finite rate of heat transfer limits the maximum obtainable power $\mathcal{P}$ [19]. The present Otto engine model is not an exception, showing similarities with previous studies of discrete quantum heat engines [5,6,10,11].

The irreversibility caused by the finite-time duration on the *adiabats* is the main finding of the present study as well as the preceding short letter [4]. This irreversibility is closely linked to the quantum adiabatic condition. The nonadiabatic parameter $\xi=\dot{\omega}J/2\Omega^2$, cf. Eqs. (75) and (80), is a measure of the inability of the state to follow the energy frame. ξ vanishes when either the change in the external field is slow $\dot{\omega}\approx 0$ or the internal and external Hamiltonians commute, $J\approx 0$. The nonadiabatic irreversibility is caused by the interplay of the noncommutability of the Hamiltonian at different points along the cycle trajectory and the dephasing caused by coupling to the heat baths on the *isochores*. This is consistent with Ref. [4] where the ''friction'' losses scaled with ξ^2. The nonadiabaticity can also be characterized by an increase in the modulus of $\langle\hat{\mathbf{L}}_{\pm}\rangle$ on the *adiabats*. Dephasing, i.e., expo-

nential decay of the modulus of $\langle \hat{\mathbf{L}}_{\pm} \rangle$ is induced by the coupling to the baths on the *isochores*.

The dynamics of the $\hat{\mathbf{L}}_{\pm}$ operator associated with the phase can be compared to the $\hat{\mathbf{B}}_{\pm}$ operator associated with the internal correlation between the spins [cf. Eq. (62)]. The absolute value of $|\hat{\mathbf{B}}_{\pm}|$ oscillates on all branches of the cycle never reaching zero. This is not surprising since $\hat{\mathbf{B}}_{\pm}$ does not commute with the Hamiltonian. The ''angle'' $\phi_B = \arctan(b_3/b_2)$ is excited for small cycle times. For cycles with large time allocation on the *isochores*, ϕ_B is found to be close to zero. These observations reflect the two types of correlations between particles. A ''classical'' correlation and a quantum correlation meaning EPR [41,42] entanglement between particles. The general trend is therefore for the engine to become more classical when the cycle times become longer. In this case, the state follows the energy direction and in addition the entanglement between particles is small. Adding pure dephasing has a similar effect. A continuous measurement of energy during operation will also lead to effective pure dephasing. For short cycle times, quantum effects become important. The entropy decrease on the adiabats, which is the result of phase memory, is such an example. The quantum effect, which influences the performance, is the excess work on the *adiabat* due to the inability of the state to follow the energy direction.

ACKNOWLEDGMENTS

This research was supported by the U.S. Navy under Contract No. N00014-91-J-1498 and the Israel Science Foundation. The authors wish to thank Lajos Diosi, David Tannor, and Jeff Gordon for their continuous support and help.

APPENDIX: THE $\hat{\mathbf{F}}$ OPERATORS

The method of construction of $\hat{\mathbf{F}}_j$ is based on identifying the operators with the raising and lowering operators in the energy frame. The matrix $\mathcal{C}$ which diagonalizes the Hamiltonian becomes:

$$\mathcal{C}=\begin{pmatrix} -\sqrt{\frac{\Omega-\omega}{2\Omega}} & 0 & 0 & \sqrt{\frac{\Omega+\omega}{2\Omega}} \\ 0 & 1 & 0 & 0 \\ 0 & 0 & 1 & 0 \\ \sqrt{\frac{\Omega+\omega}{2\Omega}} & 0 & 0 & \sqrt{\frac{\Omega-\omega}{2\Omega}} \end{pmatrix}. \tag{A1}$$

Denoting $\sqrt{\Omega-\omega/2\Omega}=\mu$, and $\sqrt{\Omega+\omega/2\Omega}=\chi$, the diagonalization of the Hamiltonian matrix becomes

$$\begin{pmatrix} -\mu & 0 & 0 & \chi \\ 0 & 1 & 0 & 0 \\ 0 & 0 & 1 & 0 \\ \chi & 0 & 0 & \mu \end{pmatrix} \begin{pmatrix} \frac{\omega}{\sqrt{2}} & 0 & 0 & \frac{J}{\sqrt{2}} \\ 0 & 0 & 0 & 0 \\ 0 & 0 & 0 & 0 \\ \frac{J}{\sqrt{2}} & 0 & 0 & -\frac{\omega}{\sqrt{2}} \end{pmatrix} \times \begin{pmatrix} -\mu & 0 & 0 & \chi \\ 0 & 1 & 0 & 0 \\ 0 & 0 & 1 & 0 \\ \chi & 0 & 0 & \mu \end{pmatrix} = \begin{pmatrix} -\frac{\Omega}{\sqrt{2}} & 0 & 0 & 0 \\ 0 & 0 & 0 & 0 \\ 0 & 0 & 0 & 0 \\ 0 & 0 & 0 & \frac{\Omega}{\sqrt{2}} \end{pmatrix}. \tag{A2}$$

In the *adiabats*, the energy frame is time dependent, therefore the equation of motion contains an additional generator:

$$\mathcal{L}_e(\hat{\boldsymbol{\rho}}_{\mathbf{e}}) = -\mathcal{C}\dot{\mathcal{C}}\hat{\boldsymbol{\rho}}_{\mathbf{e}} - \hat{\boldsymbol{\rho}}_{\mathbf{e}}\dot{\mathcal{C}}\mathcal{C} = i\frac{\dot{\omega}J}{2\Omega^2}[\hat{\mathbf{B}}_{\mathbf{3}}, \hat{\boldsymbol{\rho}}_{\mathbf{e}}]. \tag{A3}$$

On the *isochores* $\hat{\mathbf{h}}$ is time independent. The lowering transition rates $k_{\downarrow}$ are chosen to be equal for all the four transitions, while the raising transitions $k_{\uparrow}$ comply with detailed balance. Schematically, the eight transitions are

$$\begin{array}{cccccccc} \hat{\mathbf{F}}_{\mathbf{1}} & \hat{\mathbf{F}}_{\mathbf{2}} & \hat{\mathbf{F}}_{\mathbf{3}} & \hat{\mathbf{F}}_{\mathbf{4}} & \hat{\mathbf{F}}_{\mathbf{5}} & \hat{\mathbf{F}}_{\mathbf{6}} & \hat{\mathbf{F}}_{\mathbf{7}} & \hat{\mathbf{F}}_{\mathbf{8}} \\ E_2 & E_2 & E_3 & E_3 & E_4 & E_4 & E_4 & E_4 \\ \Uparrow & \Downarrow & \Uparrow & \Downarrow & \Uparrow & \Downarrow & \Uparrow & \Downarrow \\ E_1 & E_1 & E_1 & E_1 & E_2 & E_2 & E_3 & E_3. \end{array} \tag{A4}$$

Detailed presentation of a few $\hat{\mathbf{F}}_{\mathbf{i}}$ operators

The $\hat{\mathbf{F}}$ operator for the transition E_1 to E_2 is $\hat{\mathbf{F}}_{\mathbf{1\to 2}} \equiv \hat{\mathbf{F}}_{\mathbf{1}}$. In the energy picture, it is simply:

$$\hat{\mathbf{F}}_1 = \sqrt{k_{\downarrow}} \begin{pmatrix} 0 & 0 & 0 & 0 \\ 1 & 0 & 0 & 0 \\ 0 & 0 & 0 & 0 \\ 0 & 0 & 0 & 0 \end{pmatrix}. \tag{A5}$$

Using the matrix $\mathcal{C}$ to transform back to the polarization picture leads to

$$\hat{\mathbf{F}}_1=\sqrt{k_\downarrow}\begin{pmatrix}-\mu & 0 & 0 & \chi\\ 0 & 1 & 0 & 0\\ 0 & 0 & 1 & 0\\ \chi & 0 & 0 & \mu\end{pmatrix}\begin{pmatrix}0 & 0 & 0 & 0\\ 1 & 0 & 0 & 0\\ 0 & 0 & 0 & 0\\ 0 & 0 & 0 & 0\end{pmatrix}\times\begin{pmatrix}-\mu & 0 & 0 & \chi\\ 0 & 1 & 0 & 0\\ 0 & 0 & 1 & 0\\ \chi & 0 & 0 & \mu\end{pmatrix}=\sqrt{k_\downarrow}\begin{pmatrix}0 & 0 & 0 & 0\\ -\mu & 0 & 0 & \chi\\ 0 & 0 & 0 & 0\\ 0 & 0 & 0 & 0\end{pmatrix} \tag{A6}$$

Thus, $\hat{\mathbf{F}}_\mathbf{1}^\dagger$ will be

$$\hat{\mathbf{F}}_\mathbf{1}^\dagger=\sqrt{k_\downarrow}\begin{pmatrix}-\mu & 0 & 0 & \chi\\ 0 & 1 & 0 & 0\\ 0 & 0 & 1 & 0\\ \chi & 0 & 0 & \mu\end{pmatrix}\begin{pmatrix}0 & 1 & 0 & 0\\ 0 & 0 & 0 & 0\\ 0 & 0 & 0 & 0\\ 0 & 0 & 0 & 0\end{pmatrix}\times\begin{pmatrix}-\mu & 0 & 0 & \chi\\ 0 & 1 & 0 & 0\\ 0 & 0 & 1 & 0\\ \chi & 0 & 0 & \mu\end{pmatrix}=\sqrt{k_\downarrow}\begin{pmatrix}0 & -\mu & 0 & 0\\ 0 & 0 & 0 & 0\\ 0 & 0 & 0 & 0\\ 0 & \chi & 0 & 0\end{pmatrix}. \tag{A7}$$

Using a similar procedure, all the $\hat{\mathbf{F}}_\mathbf{i}$ in the polarization picture become

$$\hat{\mathbf{F}}_\mathbf{1}=\hat{\mathbf{F}}_{1\to 2}=\sqrt{k_\downarrow}\begin{pmatrix}0 & 0 & 0 & 0\\ -\mu & 0 & 0 & \chi\\ 0 & 0 & 0 & 0\\ 0 & 0 & 0 & 0\end{pmatrix}, \tag{A8}$$

$$\hat{\mathbf{F}}_\mathbf{2}=\hat{\mathbf{F}}_{2\to 1}=\sqrt{k_\uparrow}\begin{pmatrix}0 & -\mu & 0 & 0\\ 0 & 0 & 0 & 0\\ 0 & 0 & 0 & 0\\ 0 & \chi & 0 & 0\end{pmatrix}, \tag{A9}$$

$$\hat{\mathbf{F}}_\mathbf{3}=\hat{\mathbf{F}}_{\mathbf{1}\to\mathbf{3}}=\sqrt{k_\downarrow}\begin{pmatrix}0 & 0 & 0 & 0\\ 0 & 0 & 0 & 0\\ -\mu & 0 & 0 & \chi\\ 0 & 0 & 0 & 0\end{pmatrix}, \tag{A10}$$

$$\hat{\mathbf{F}}_\mathbf{4}=\hat{\mathbf{F}}_{3\to 1}=\sqrt{k_\uparrow}\begin{pmatrix}0 & 0 & -\mu & 0\\ 0 & 0 & 0 & 0\\ 0 & 0 & 0 & 0\\ 0 & 0 & \chi & 0\end{pmatrix}, \tag{A11}$$

$$\hat{\mathbf{F}}_\mathbf{5}=\hat{\mathbf{F}}_{\mathbf{2}\to\mathbf{4}}=\sqrt{k_\downarrow}\begin{pmatrix}0 & \chi & 0 & 0\\ 0 & 0 & 0 & 0\\ 0 & 0 & 0 & 0\\ 0 & \mu & 0 & 0\end{pmatrix}, \tag{A12}$$

$$\hat{\mathbf{F}}_\mathbf{6}=\hat{\mathbf{F}}_{\mathbf{4}\to\mathbf{2}}=\sqrt{k_\uparrow}\begin{pmatrix}0 & 0 & 0 & 0\\ \chi & 0 & 0 & \mu\\ 0 & 0 & 0 & 0\\ 0 & 0 & 0 & 0\end{pmatrix}, \tag{A13}$$

$$\hat{\mathbf{F}}_\mathbf{7}=\hat{\mathbf{F}}_{\mathbf{3}\to\mathbf{4}}=\sqrt{k_\downarrow}\begin{pmatrix}0 & 0 & \chi & 0\\ 0 & 0 & 0 & 0\\ 0 & 0 & 0 & 0\\ 0 & 0 & \mu & 0\end{pmatrix}, \tag{A14}$$

$$\hat{\mathbf{F}}_\mathbf{8}=\hat{\mathbf{F}}_{\mathbf{4}\to\mathbf{3}}=\sqrt{k_\uparrow}\begin{pmatrix}0 & 0 & 0 & 0\\ 0 & 0 & 0 & 0\\ \chi & 0 & 0 & \mu\\ 0 & 0 & 0 & 0\end{pmatrix}. \tag{A15}$$

[1] S. Carnot, *Réflections sur la Puissance Motrice du Feu et sur les Machines Propres à Développer Cette Puissance* (Bachelier, Paris, 1824).
[2] L. Szilard, Z. Phys. **53**, 840 (1929).
[3] Leon Brillouin, *Science and Information Theory* (Academic Press, New York, 1956).
[4] R. Kosloff and T. Feldmann, Phys. Rev. E **65**, 055102 (2002).
[5] T. Feldmann, E. Geva, R. Kosloff, and P. Salamon, Am. J. Phys. **64**, 485 (1996).
[6] T. Feldmann and R. Kosloff, Phys. Rev. E **61**, 4774 (2000).
[7] S. Lloyd, Phys. Rev. A **56**, 3374 (1997).
[8] J. Geusic, E.S. du Bois, R.D. Grasse, and H. Scovil, J. Appl. Phys. **30**, 1113 (1959).
[9] R. Kosloff, J. Chem. Phys. **80**, 1625 (1984).
[10] E. Geva and R. Kosloff, J. Chem. Phys. **96**, 3054 (1992).
[11] E. Geva and R. Kosloff, J. Chem. Phys. **97**, 4398 (1992).
[12] E. Geva and R. Kosloff, J. Chem. Phys. **104**, 7681 (1996).
[13] J.C. Chen, B.H. Lin, and B. Hua, J. Phys. D **35**, 2051 (2002).
[14] C.M. Bender, D.C. Brody, and B.K. Meister, J. Phys. A **33**, 4427 (2000).
[15] C.M. Bender, D.C. Brody, and B.K. Meister, Proc. R. Soc. London, Ser. A **458**, 1519 (2002).

[16] R. Kosloff, E. Geva, and J.M. Gordon, J. Appl. Phys. **87**, 8093 (2000).
[17] J.P. Palao, R. Kosloff, and J.M. Gordon, Phys. Rev. E **64**, 056130 (2001).
[18] E. Geva, J. Mod. Opt. **49**, 635 (2002).
[19] F.L. Curzon and B. Ahlborn, Am. J. Phys. **43**, 22 (1975).
[20] A. Ben-Shaul and R.D. Levine, J. Non-Equilib. Thermodyn. **4**, 363 (1979).
[21] P. Salamon, J.D. Nulton, G. Siragusa, T.R. Andersen, and A. Limon, Energy (Oxford) **26**, 307 (2001).
[22] P. Salamon, A. Nitzan, B. Andresen, and R.S. Berry, Phys. Rev. A **21**, 2115 (1980).
[23] J.M. Gordon and M. Huleihil, J. Appl. Phys. **69**, 1 (1991).
[24] B. Andresen, *Finite-Time Thermodynamics* (Phys. Lab II. University of Copenhagen, Copenhagen, 1983).
[25] A. Bejan, *Entropy Generation Minimization* (Chemical Rubber Corporation, Boca Raton, FL, 1996).
[26] K.C. Ng, H.T. Chua, K. Tu, J.M. Gordon, T. Kashiwagi, A. Akisawa, and B.B. Saha, J. Appl. Phys. **83**, 1831 (1998).
[27] K. Lendi and A.J. van Wonderen, J. Phys. A **34**, 1285 (2001).
[28] G. Lindblad, Commun. Math. Phys. **48**, 119 (1976).
[29] Y. Alhassid and R.D. Levine, Phys. Rev. A **18**, 89 (1978).
[30] B.G. Adams, J. Cizek, and J. Paldus, Adv. Quantum Chem. **19**, 1 (1988).
[31] B.G. Wybourne, *Classical Groups for Physics* (Wiley, New York, 1973).
[32] R. Alicki and K. Lendi, *Quantum Dynamical Semigroups and Applications* (Springer-Verlag, Berlin, 1987).
[33] H. Spohn and J.L. Lebowitz, Adv. Chem. Phys. **38**, 109 (1979).
[34] R. Alicki, J. Phys. A **12**, L103 (1979).
[35] A. Wehrl, Rev. Mod. Phys. **50**, 221 (1978).
[36] Allon Bartana, Ronnie Kosloff, and David J. Tannor, J. Chem. Phys. **99**, 196 (1993).
[37] J. Wei and E. Norman, Proc. Am. Math. Soc. **15**, 327 (1963).
[38] P. Carruthers and M.M. Nieto, Rev. Mod. Phys. **40**, 411 (1968).
[39] J.M. Levyleblond, Ann. Phys. (N.Y.) **101**, 319 (1976).
[40] G. Gour, Found. Phys. **32**, 907 (2002).
[41] A. Einstein, B. Podolsky, and N. Rosen, Phys. Rev. **47**, 777 (1935).
[42] G. Lindblad, Commun. Math. Phys. **33**, 305 (1973).
[43] K.H. Hoffmann, Ann. Phys. (N.Y.) **10**, 79 (2001).